Control of a Subsea Multiphase Boosting Station

Harish Satyavada

Master of Science Thesis

TU Delft Delft University of Technology

Delft Center for Systems and Control

Control of a Subsea Multiphase Boosting Station

Master of Science Thesis

For the degree of Master of Science in Systems and Control at Delft University of Technology

Harish Satyavada

June 15, 2016

Faculty of Mechanical, Maritime and Materials Engineering (3mE) · Delft University of Technology

The work in this thesis was supported by GE Global Research. Their cooperation is hereby gratefully acknowledged.

Abstract

Subsea multiphase boosting is a technology that is gaining interest from oil & gas operators and suppliers. In response to the growing interest in multiphase boosting technology, GE is working on the development of a subsea multiphase boosting station. In this work, controller synthesis needs are identified for safe and reliable operation of the boosting station.

In order to implement and validate control strategies pertaining to the multiphase pump and subsea boosting station, an integrated co-simulation environment is used. After estimating certain process parameters, various control strategies are developed to meet the control objectives. The strategies are distinguished based on sensor requirements, implementation difficulty, efficiency and expected production. Performance of the controllers are tested in the most severe conditions the boosting station may be subjected to. Finally, sensitivity analysis is done to test the control strategies in the presence of uncertainties.

Table of Contents

List of Figures

List of Tables

Acknowledgements

I would like to express my deep gratitude to my supervisor and mentor Dr. Rosa Castane Selga for her assistance during the writing of the thesis and also for the constant guidance she provided me which enabled me to achieve the set goals. I am indebted to my professor Dr. Simone Baldi who has constantly steered me in the right direction during the thesis and my master's study. Special thanks to the committee members for patiently going through the work and acknowledging it.

I am grateful for the love and encouragement from Monica Avala. Without her patience and sacrifice, I could not have completed this thesis. Last but not the least, I would like to thank my family for their continuous support and motivation.

Delft, University of Technology — Harish Satyavada
June 15, 2016

Chapter 1

Introduction

Subsea multiphase boosting is a technology that is gaining interest from oil & gas operators and suppliers, offering robust and effective means to improve production from new or ageing reservoirs [2]. In response to the growing interest in multiphase boosting technology, GE is working on the development of a subsea multiphase boosting station. The components of the boosting station have interactions among themselves as well as with the whole production system including upstream and downstream flowlines and risers.

The oil and gas reservoirs (wells) are located below the seabed. The well consists of a long horizontal section (several kilometres). The wellhead is shown as a red dot on the surface in Fig. 1-1. The upstream flowline consists of the well and its production area, the wellhead and the pipe to the inlet of the subsea boosting station. Ths subsea boosting station is located on the seabed. The inlet of the subsea boosting station is connected to the upstream flowline on the rightmost position in Fig. 1-1.

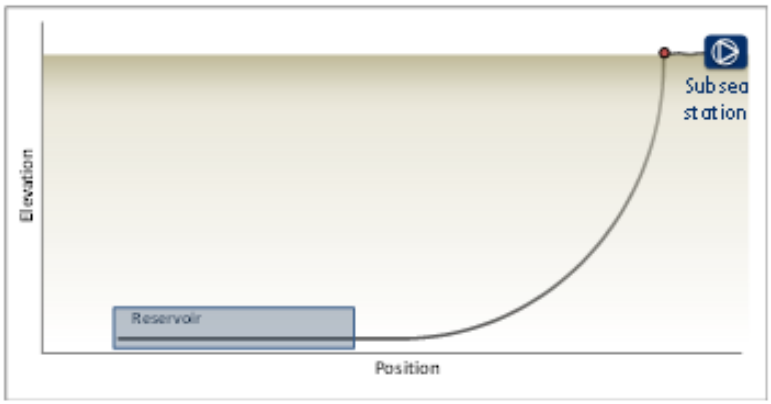

Figure 1-1: Well and upstream flowline.

The oil and gas production from the boosting station is extracted to a level above the surface of the sea. The downstream flowline is typically long (several kilometres) and negatively

inclined. It also consists of an almost horizontal section followed by a riser (refer Fig. 1-2). A riser system is essentially a conductor pipe connected to the top-side facility above the sea surface. In the model under consideration, use is made of an S-shaped riser for the production riser [3]. The function of the topside facilities is to separate the production fluid into separate phases (gas, oil and water), and process these phases into marketable products or dispose them in an environmentally acceptable manner [1].

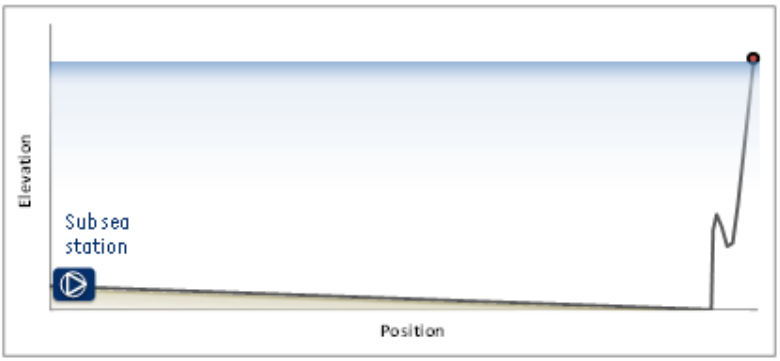

Figure 1-2: Donwstream flowline and S-Shaped risers.

1-1 The subsea multiphase boosting station

1-1-1 The layout

The layout of the boosting station considered is given in Fig. 1-3. The two wells are connected to the boosting station via upstream flowlines. The inlet device at the boosting station is typically a mixer. The boosting station consists of two multiphase pumps (MPP 1,2). Also, a recirculation loop is present which is regulated by the recirculation valve/choke. The outlet device (usually a separator) is connected to downstream flowlines followed by the risers. The risers are connected to the topside facilities.

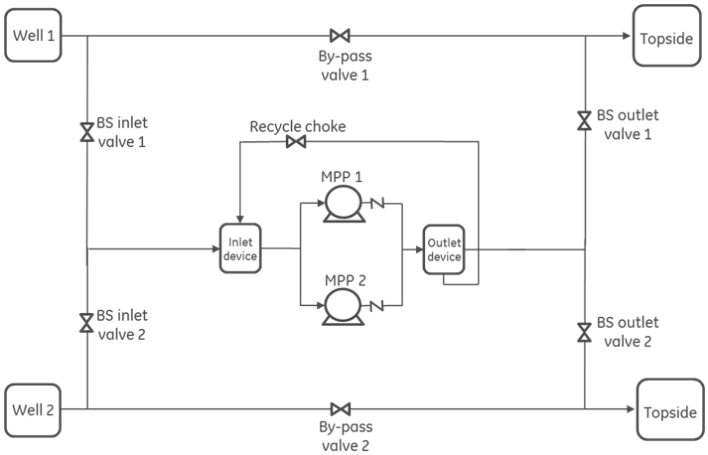

Figure 1-3: Layout of the boosting station.

1-1-2 Sensors and actuators

Sensors present in the boosting station and the parameters measured by them are listed are listed in Table 1-1. The sensor at the outlet of the inlet device is a Multiphase flowmeter (MPFM). This sensor is optional and dependent on the customer needs/expectation.

Table 1-1: Sensors present in the boosting station

Location	Sensing parameter
BS valve-1 inlet and outlet	Pressure
BS valve-2 inlet and outlet	Pressure
Recycle choke inlet and outlet	Pressure
MPP 1,2 inlet and outlet	Pressure
MPP 1,2	Speed and power consumed
Inlet device outlet (red dot in Fig. 1-3)	Gas volume fraction (GVF) and volume flow

The actuators present in the system are:

1. Control signal to the recirculation valve. Range: [5 100] %, minimum 5% to prevent hydrates formation.
2. Pump speeds of MPP 1 & 2. Range: [2000 6000] rpm.

1-1-3 The multiphase pump technology

Multiphase pumping essentially consists adding hydraulic energy to an unprocessed production stream [4]. The ability to boost multiphase fluids implies a number of advantages like: increased flowrate in an existing export pipe-line, production of low-pressure wells in a common high-pressure processes, production of reserves from economically marginal fields.

Multiphase pumping is realized by a multiphase pump in our case. The multiphase pump is a key component of the boosting station. The first effective multiphase pumps (MPP) for oilfield production use were demonstrated in the 1970s [5]. The development of multiphase pump technology marked by a number of test projects and successful results paved the way to its effective use today [6].

Multiphase pumping eliminates equipment such as separators, compressors, pumps, flares and allows the centralization of processing facilities [7]. The multiphase pump is essentially a multi-stage pump [8] which tolerates a high amount of gas at its inlet, thereby eliminating the requirement for separation and transit via two separate flow lines. This flexible solution is however subject to novel challenges linked to the monitoring and control of gas volume fraction (GVF) variations caused by the well and upstream flowlines. For safe and reliable functioning of the multiphase pump, it is critical to maintain the GVF at pump inlet below its specification limit and also ensure that there is a minimum volume flow into the pump [9].

This need essentially drives for controls for the multiphase pumps. As such, controls for multiphase pumps are not commonly available in literature. Therefore, we make use of literature related to compressor controls. The multiphase pumps are after all hybrid machines somewhere between compressors and pumps.

1-2 Review on turbomachinery controls

Turbomachinery describes machines that transfer energy between a rotor and a fluid, including both turbines and compressors. In a centrifugal compressor, energy is transferred from a set of rotating impeller blades to the gas. Common control strategies pertaining to the compressors are:

- **Anti surge control:** Anti surge control is common in compressor controls. Surge is a condition that occurs on compressors when the amount of gas they are trying to compress is insufficient for the speed of the compressor and the turbine blades lose their forward thrust, causing a reverse movement in the shaft. This condition can have catastrophic effects on the machine, so compressor manufacturers include anti-surge valves that recycle gas from the discharge to the suction when a low flow is detected. Usually these valves are designed to be only open on startup or under reduced rates [10].
- **Load sharing:** The complexity of load sharing compressors in petrochemical or pipeline applications can be challenging. However, advanced performance control algorithms are designed to share key compressor state, load, and operation information, allowing the overall system to be optimized and to proactively respond to large or small process changes [11].

The concepts of anti surge control and load sharing control can be adopted to design controls for the multiphase pumps. However, designing controls for the safe and reliable operation of the multiphase pumps and the boosting station is more complicated and challenging as described in the following section.

1-3 Challenges pertaining to mutliphase boosting station controls

- **Gas volume fraction:** Compressors are capable of handling pure gas (100% GVF) and pumps do not handle gases (0% GVF). The multiphase pumps however handle both gas and liquids, but there is a hard limitation on the GVF they can handle. The GVF handling limitation for the multiphase pumps under our consideration is 80%. It is mandatory to make sure that the GVF at the multiphase pumps inlet is less than 80%.
- **Limited sensor information:** Operators dealing with compressor controls have the GVF and volume flow measurements available. However, as shown in Table 1-1 the sensors in the multiphase boosting station are limited. Particularly, the availability of MPFM sensor for GVF and volume flow is uncertain. This calls for estimation of GVF and other parameters required to design controls for the boosting station.

- **Uncertainty:** The operating points of multiphase pumps are characterized by pump maps. The current operating point in a pump map depends on the pressure head, volume flow, GVF at the pump inlet and current operating speed of the MPP. In an ideal scenario, it is expected that the reservoir volume flow splits identically into either of the multiphase pumps. Therefore both the multiphase pumps are expected to operate at the same point in the pump maps. However, in reality it is more likely that the reservoir volume flow is not equally split across the MPPs. Some of the possible reasons for an asymmetric split of the reservoir flow are:

  1. The mechanical construction of the pumps.
  2. Pumps located at different altitudes: Relatively the two pumps in the boosting station may be located at different altitudes. As a result, the suction pressure across each pump will be will be slightly different, leading to an asymmetric split.
  3. Clogging of pipelines: Clogging of pipes is a natural phenomenon. It occurs due to limescale formation in the pipes over time. As a result, it is possible that the volume flow rate of the fluids into the MPPs is different from each other.

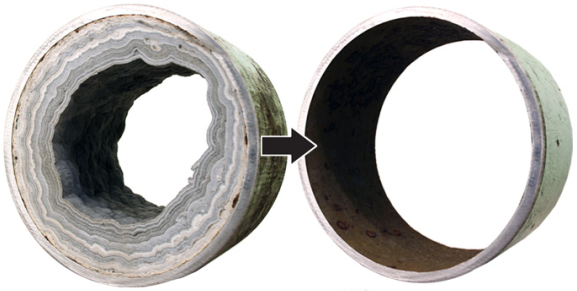

Figure 1-4: Clogging of a pipeline

- **Slugs:** Slugs are characterized by a series of liquid plugs separated by relatively large gas pockets [1]. Slug flow patterns occurring in multiphase horizontal and vertical flow lines are shown in Fig. 1-5.

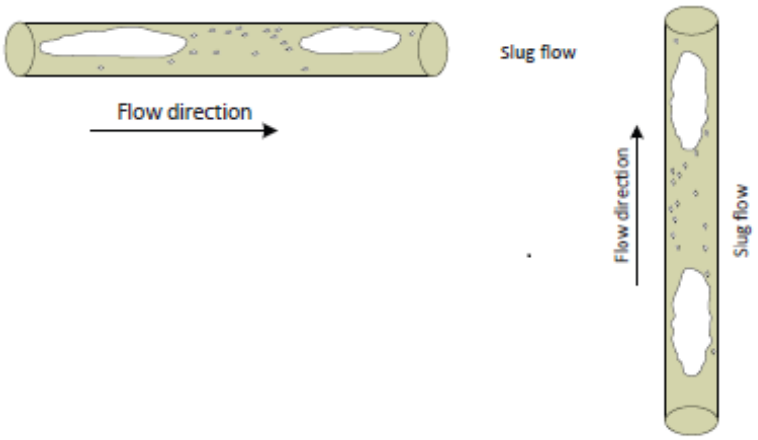

Figure 1-5: Slug flow patterns in horizontal and vertical flow lines (edited from [1])

Two kinds of slugs are commonly prevalent which pose a risk to the safety and performance of the boosting station and the risers:

1. Reservoir slugs: The occurrence of slugs is commonly prevalent in oil and gas wells. The large gas packets constituting the slugs have a GVF of 100%. In the absence of proper controls, such slugs tend to have a catastrophic effect on the safety and functioning of the multiphase pumps.
2. Riser slugging: Slugging in production risers has for many years been a major operational problem in subsea oil & gas fields developments [12]. Literature pertaining to eliminating slugging in production risers consider: increase of pressure at the separator at the top-side facility to stabilize the unstable flow [13], [14], gas lift technique to suppress flow intermittency [15], controlling the top-side choke located at the top of the riser [16], [17] and operation of a control valve at riser base instead of top-side [18]. As control of the top-side choke and facility is considered out of scope, an alternative control strategy is to be designed to eliminate riser slugging.

1-4 Control objectives

Bearing in mind the challenges and concerns raised in 1-3, the following control objectives are identified which are to be addressed in this thesis:

- **Master control**: The user may specify the demand in terms of desired values of the process variables pertaining to: discharge pressure at pump outlet, suction pressure at pump inlet and production fluid mass flow at mixer outlet. It is necessary to design a master controller that controls the demand and ensures general safety of the boosting station.
- **Load sharing**: The subsea multiphase boosting station consists of two multiphase pumps. Each of these two pumps boost the reservoir flow. As these pumps operate parallely, it is mandatory to ensure that the load (reservoir flow) is balanced between the pumps.
- **Minimum flow & GVF control**: For the safety of the multiphase pumps, it is essential to ensure that minimum flow into the pump and maximal GVF at the pump inlet are not violated. While the minimum flow controller is to make sure that there is a minimum volume flow into the pumps to avoid surge, the GVF controller is to ensure that the GVF at the inlet of the pumps is always under the prescribed limit.
- **Riser slugging control**: In order to mitigate riser slugging and ensure constant production, an anti-slug controller has to be designed for the riser slugging phenomenon.

In order to implement and validate control strategies pertaining to the multiphase pump and subsea boosting station, an integrated co-simulation environment was used. The integrated co-simulation environment consists of: K-Spice for process simulation, LedaFlow for multiphase flow line simulation, Simulink for rapid prototyping of control algorithms, and MatrikonOPC [19] for real-time, bidirectional data exchange between the process model and its controls [2].

1-5 Outline of the thesis

The remainder of the thesis is organized as follows: Chapter 2 contains the description of the simulation environment, Chapter 3 describes the estimation scheme used to estimate GVF and reservoir volume flow, Chapter 4 deals with synthesizing of controllers addressing the control objectives, Chapter 5 presents the worst case scenario simulations and sensitivity analysis and in Chapter 6 conclusions and future scope are listed.

Chapter 2

The Simulation Environment

2-1 Definition of the scenario

The system model consisting of the upstream, downstream flowlines, oil and gas wells, boosting station and the S shaped risers are based on the Schiehallion oil field. The Schiehallion field is located 150 km west of Shetland and has a water depth of 400 m. This oil field has been in production since 1998.

The parameters and geometry pertaining to the whole production system (system model) are fixed based on a case study on the Schiehallion oil field done by GE oil & gas [20]. Some of the parameters are described in Table 2-1.

Table 2-1: Production system parameters from Schiehallion case study.

Parameter description	Value
Well depth	1750 m
Well production area length	2000 m
Reservoir pressure	Hydrostatic, 225 bar
Upstream pipeline diameter	around 0.19 m
Downstream flowline length	4000 m
S shaped riser elevation	400 m

In order to accurately capture the interactions between the subsea multiphase boosting station and the flowlines connected to it, a process simulator (K-Spice) is linked to a multiphase pipe flow simulation tool (LedaFlow). This integrated solution is subsequently linked to Matlab/Simulink for the development of control strategies.

2-2 LedaFlow

LedaFlow is a multiphase pipe flow simulator. The upstream, downstream flowlines and the wells have been modelled using LedaFlow. The LedaFlow model also includes the top side choke.

2-3 The K-Spice model

The subsea boosting station is modelled in K-Spice. K-Spice is a fully dynamic process simulator developed by Kongsberg which is used to model all components inside the multiphase boosting station. As it can be observed from Fig. 2-1, the key components of the boosting station are oil & gas reservoirs, Multiphase pumps (MPP-1 and MPP-2), Mixer, Separator, Recirculation valve, Bypass Valve, Production risers and topside choke. These components are described in the following subsections.

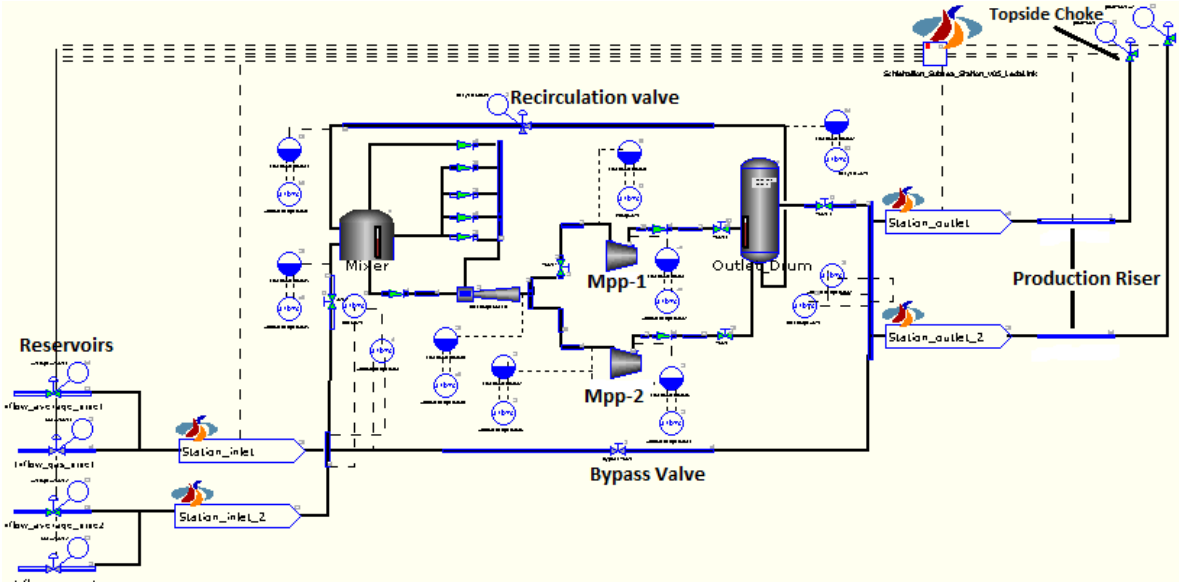

Figure 2-1: Subsea boosting station model in K-Spice.

2-3-1 Oil and gas reservoirs and upstream flowlines

The parameters of the reservoir and well production area are implemented in a Ledaflow model. It is linked to the K-Spice model for realistic behavior. The reservoir model in K-Spice consists of average and gas valves (refer Fig. 2-2) to simulate a typical oil and gas reservoir. From the average valve, an average composition of oil and gas mixture is obtained. From the gas valve, pure gas (100% GVF) is obtained. The reservoir is connected to the boosting station through upstream flowlines.

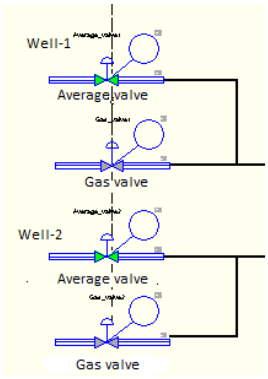

Figure 2-2: Well model in K-Spice.

2-3-2 Mixer

The mixer or slug catcher is designed to ensure passive safety of the multiphase pump. In case of any strong variations at the boosting station inlet, the mixer is designed so as to limit both rate of change and absolute value of GVF at the pump inlet [2].

The mixer acts as a buffer to protect the pump from these GVF variations. The buffer function is achieved since the slug catcher contains a given amount of gas and liquid during normal operations. The tank is self-regulating in the sense that the GVF of its outlet will depend on the relative amount of gas and liquid in the tank. If a large pocket of gas enters the system, the liquid level in the tank will slowly decrease, and so will the GVF at the outlet. It also serves as a flow pre-conditioning unit to feed the pump with a high quality homogeneous flow. The mixer is also in contact with the recirculation flow so as to mix the reservoir flow with the recirculated liquid.

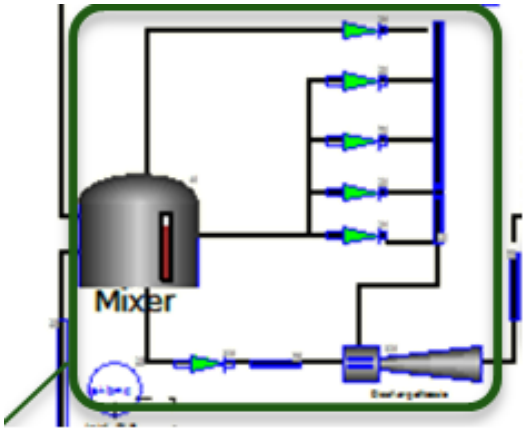

Figure 2-3: Mixer model in K-Spice.

2-3-3 Multiphase pump

Multiphase pumps are capable of increasing the pressure of a multiphase stream thereby making them a key component of the boosting station. This allows increasing production and recovery on existing field or enabling an economic development of new fields with long step-out. The key characteristics that need to be captured while modelling the MPPs are:

- **Pump maps**: Pump maps or Performance maps contain information on head delivered by the pump based on volume flow, GVF at pump inlet and speed.
- **Minimum and Maximum flow**: Depending on pump speed and GVF, the minimum and maximum flow limit in a pump is determined. This helps in finding the surge and stonewall boundaries.
- **Limit on Speed**: It is important to limit the pump speed to an acceptable range depending on the GVF in order to avoid excessive pressure increase at lower gas fractions.
- **Inertia and Motor characteristics**: Pump inertia and motor characteristics are important in order to accurately capture the dynamic response of the pump.

Multiphase pumps are not available in most process simulation tools yet. A recent update in K-Spice now allows the user to implement three-dimensional maps in a compressor module, allowing the user to give a head/volume flow relationship for different speed, GVF and another parameter depending on the users' choice. This flexibility and true multi-dimensional interpolation in the definition of the performance map allows a stable interpolation in all the dimensions needed for accurately representing the characteristics of a multiphase pump.

A multiphase pump will typically operate in GVF that can range from 0% to 100%. However for pump safety 80% is fixed as a hard limitation.

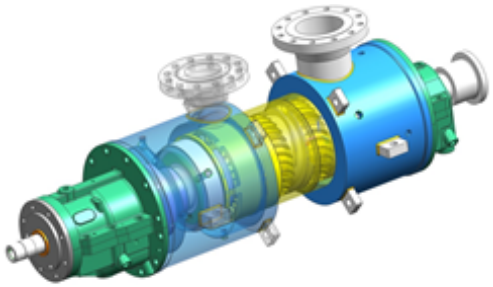

Figure 2-4: A multiphase pump.

Multiphase pumps are typically characterized by static pump maps or performance maps.

2-3-3-1 Pump maps

The multiphase pump maps or performance maps used in the dynamic simulations describe the relationship between the actual inlet volumetric flow rate, pressure head at different pump rotational speed and inlet GVFs.

The pump maps are defined for rotational speeds of 2000, 3000, 4000, 5000 and 6000 RPM for GVF values of 0, 30, 40, 50, 60, 70, 80 and 90 %. If the GVF at the pump inlet is in between the given GVF values, K-Spice interpolates the pump maps for the current GVF value.

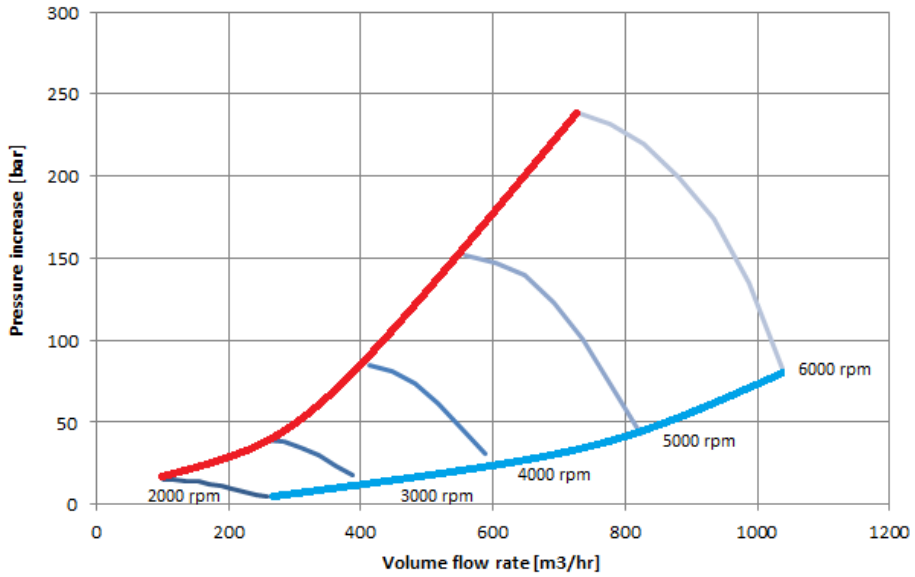

Figure 2-5: Typical pump map for the multiphase pump.

In Fig. 2-5 a typical pump map is shown. A pump map is specific to a particular GVF and it consists of various speed lines depending on the pump operation speed. Further the operating point in the pump maps changes also with volumetric flow rate of the mixture at pump inlet (x axis) and differential pressure across the pump (y axis). The red line in Fig. 2-5 is the minimal volume flow line or also known as the surge line. For safe pump operation, we should operate at a point right of the surge line and at the same time ensure the GVF at pump inlet is less than the specified limit. The light blue line is the stonewall or choke line and it is advised to operate the pump in such a way that we are to the left of the choke line. Further, it can be observed that the pump maps are highly nonlinear thereby imposing additional control related challenges.

2-3-4 Separator and recirculation loop

For long-term protection of the MPP a separator is provided in combination with a recycle loop. The separator contains liquid in the bottom, which is recirculated when the recirculation valve is open. If the recirculation valve is closed, the separator will not have any large effect on the process when the liquid level in it is stable.

The function of the recycle loop is to recirculate a fraction of the pump discharge back to the inlet so that the pump is able to maintain an acceptable GVF at its inlet during an extended period of inlet gas slugs. The efficiency of this mechanism is further increased by using a separator device at the outlet of the pump, thereby decreasing the gas fraction of the flow being recirculated.

2-3-5 Production riser and top-side choke

Production risers are the connection between the subsea field developments and production and top-side facilities. Subsea risers are a type of pipeline developed for vertical transportation. Similar to pipelines or flowlines, risers transport produced hydrocarbons, as well as production materials, such as injection fluids, control fluids and gas lift. Usually insulated to withstand seafloor temperatures, risers can be either rigid or flexible [21]. For the system under consideration, we use S shaped risers.

The top-side choke is modelled in LedaFlow, but it can be controlled in K-Spice. A constant pressure boundary condition is imposed after this topside choke, therefore assuming the topside separator pressure can be controlled perfectly.

2-4 MATLAB: controllers synthesis

The controllers are developed in MATLAB/Simulink. Simulink aids in rapid prototyping of control algorithms and also auto-coding the control strategies to be tested by PLCs for Hardware-in-the-loop validation.

2-5 The co-simulation environment

The subsea boosting station model in K-Spice and the upstream and downstream flowline models in LedaFlow are integrated for simultaneous simulation. A link is established in K-Spice at both boundaries of the subsea stations to the corresponding LedaFlow models. Data for the pressure and flowrate is therefore exchanged between the two tools, and the operation of the subsea station influences the flow regime and properties in the flowlines, which in turn impacts the boundaries of the station.

The control strategies are developed in MATLAB/Simulink. K-Spice is OPC-compliant, which allows it to integrate with the most standard control systems and various third party tools, such as MATLAB in our case. The design and validation of controls strategies is enabled by an OPC link between K-Spice and MATLAB/Simulink using a Matrikon OPC server (refer Fig. 2-5). The Matrikon OPC aids in real-time, bidirectional data exchange between the integrated (K-Spice/LedaFlow) model and its controllers in MATLAB.

Information on the process parameters from the integrated model (K-Spice/LedaFlow) is sent to MATLAB via the OPC. For control synthesis we make use of only the process variables measured by the sensors listed in Table 1-1. The other parameters are passed only for monitoring purpose.

Likewise, we pass the actuation commands pertaining to pump speeds and recirculation valve opening from the MATLAB controllers to the integrated process model.

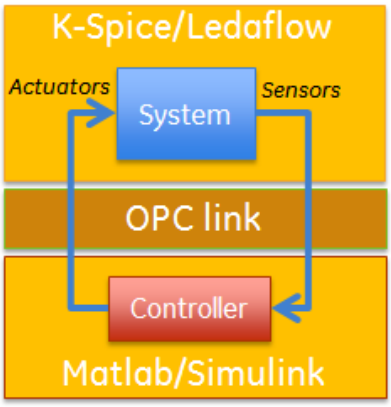

Figure 2-6: The co-simulation controller synthesis environment.

To summarize, we have setup a co-simulation environment (refer Fig. 2-7) that enables us to design and validate different control strategies in real-time against a high fidelity simulation model for the entire subsea production system, from reservoir to topside choke. The environment also enables us to evaluate trade-offs between controls, instrumentation, actuation and the system topology.

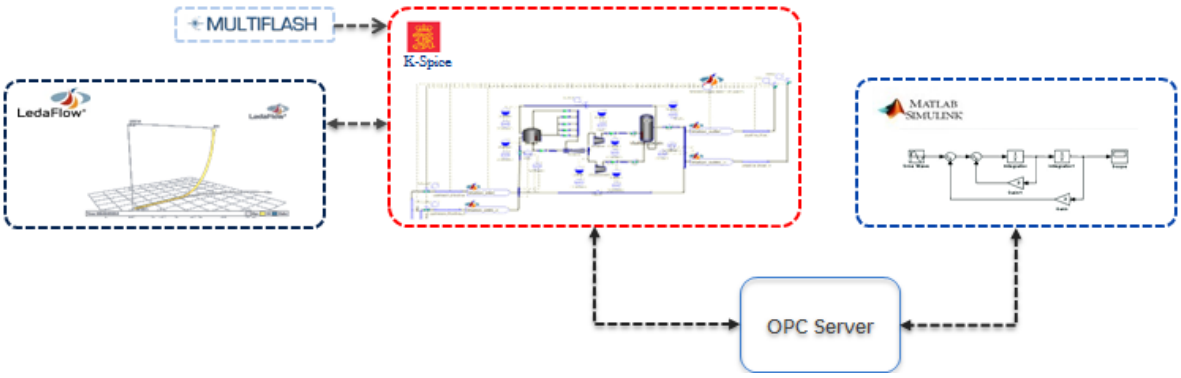

Figure 2-7: The co-simulation environment.

Chapter 3

GVF and Reservoir Volume Flow Estimation

As it can be observed from Table 1-1, the sensors available for measuring the process parameters pertaining to the boosting station are limited. For designing controllers to ensure safe and reliable operation of the boosting station, the information from the sensors is not sufficient. An estimation scheme is proposed 3-2 for estimating volume flow from the reservoirs. The estimated reservoir volume flow is used to design controllers in Chapter 3.

For the multiphase pumps, it is critical that the GVFs at the inlet of the pumps are below 80%. Information on GVFs at the inlet of the pumps is available in K-Spice which is a simulation tool. In reality, the only sensor for measuring GVF: the MPFM is an optional sensor and user dependent. Moreover, due to physical limitations related to space constraints, the MPFM can be placed only at the mixer outlet [22]. In an ideal scenario where the reservoir flow is expected to be equally split across the two pumps, the GVF at the pumps inlet is expected to be equal to the GVF measured by the MPFM placed at the Mixer outlet. However, due to the reasons listed in 1-3, it is expected that there is an asymmetric split of the reservoir flow thereby leading to different GVFs at the pump inlets with respect to the MPFM measurement. Therefore, a method to estimate GVF at the inlet of the pumps based on available measurements is proposed and evaluated in 3-1.

3-1 GVF estimation

For fault tolerant control and condition monitoring, a method for online GVF estimation from the model based on available measurements (differential pressure, pump speed, power consumed) and the pump maps is proposed in this section.

3-1-1 The estimation algorithm

The pump maps consist of a number of data points for different combinations of pressure head, pump speed, GVF and current volume flow. These data points are plotted with pump speed, differential pressure (ΔP), and power consumed constituting the x, y and z axes respectively. To be noted is that these data points consist of GVF values $\in$ [0 30 50 60 70 80 90] in [%]. A polynomial surface is fit (refer Fig. 3-1) for each GVF value using the `fit` function in MATLAB.

The model type chosen is `poly21` therefore we have a polynomial surface of degree 2 in x and degree 1 in y. In our case, the x corresponds to pump speed and y corresponds to differential pressure. The linear model `poly21` is given by:

$$P(v_P, \Delta P) = p_{00} + p_{10}v_p + p_{01}\Delta P + p_{20}v_p^2 + p_{11}\Delta P v_P, \tag{3-1}$$

where P is the current power consumed in [kW], p_{00}, p_{10}, p_{01}, p_{20} and p_{11} are the polynomial coefficients, v_p is pump speed in [rpm] and ΔP is differential pressure across the pump in [bar]. Due to space constraints, the polynomial coefficients and their confidence bounds for each of these surfaces is not shown.

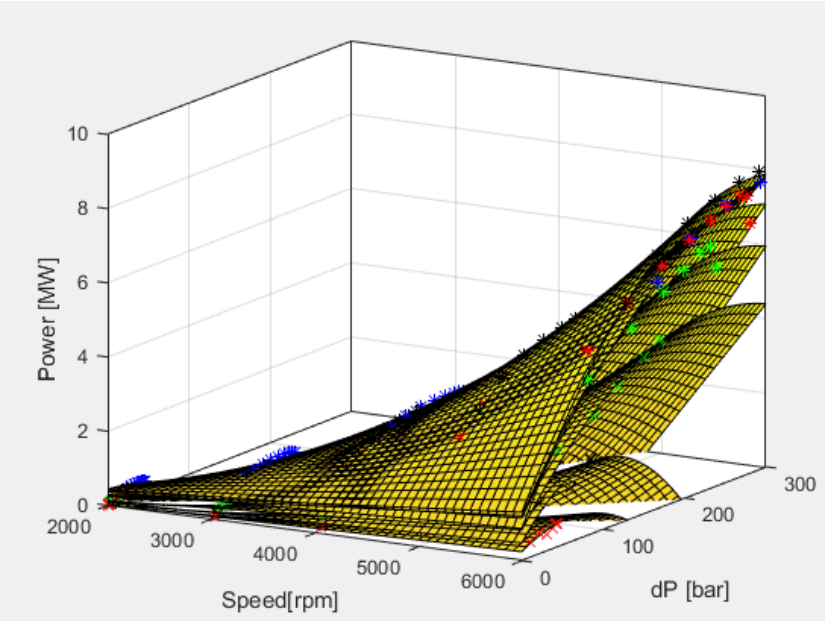

Figure 3-1: Surface fit for GVF estimation.

It is possible that the current operating point for the combination of speed, differential pressure and power lies between the GVF surfaces. For such points, the GVF must be interpolated using the known measurements and the GVF surfaces. As shown in Fig. 3-2 the current operating point lies between two GVF surfaces. It lies at a distance factor α from the lower surface and 1-α from the upper surface.

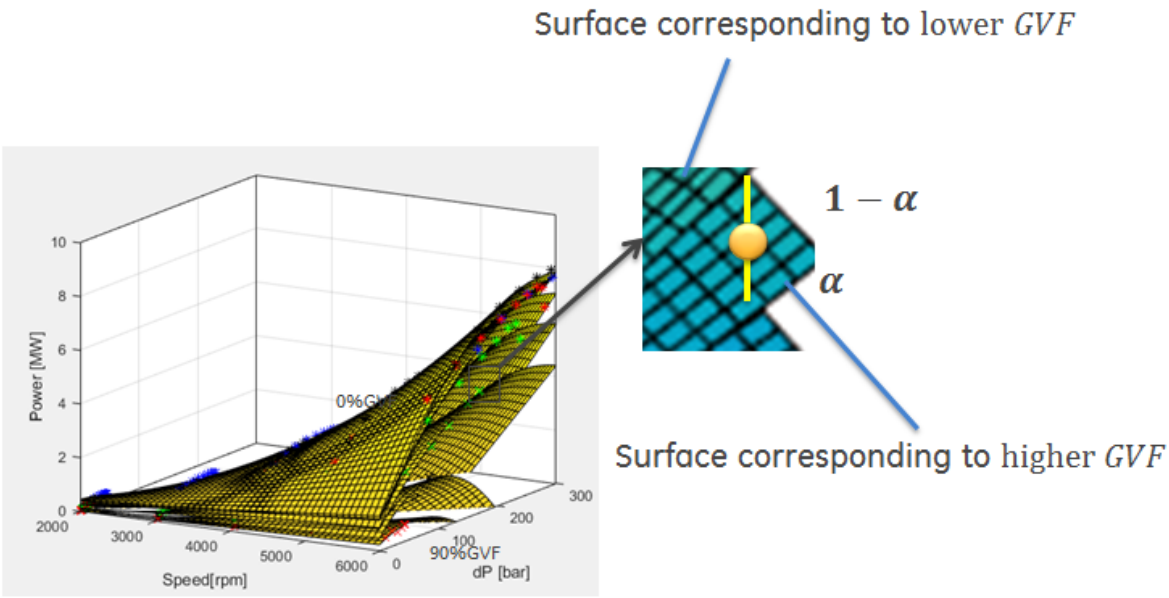

Figure 3-2: Operating point lying betwen two GVF surfaces.

The distance factor α is given by:

$$\alpha = \frac{P - P_{GVF_{low}}}{P_{GVF_{high}} - P_{GVF_{low}}}, \tag{3-2}$$

where $P_{GVF_{low}}$ is the power from the lower GVF surface and $P_{GVF_{high}}$ is the power from the higher GVF surface. Using α the GVF is estimated by:

$$GVF_{est} = \alpha(GVF_{high} - GVF_{low}) + GVF_{low}, \tag{3-3}$$

where GVF_{est} is the estimated GVF in [%]. This estimation algorithm is run online. GVF from the estimation algorithm is compared with the real GVF (obtained from Kspice) in the simulations presented below.

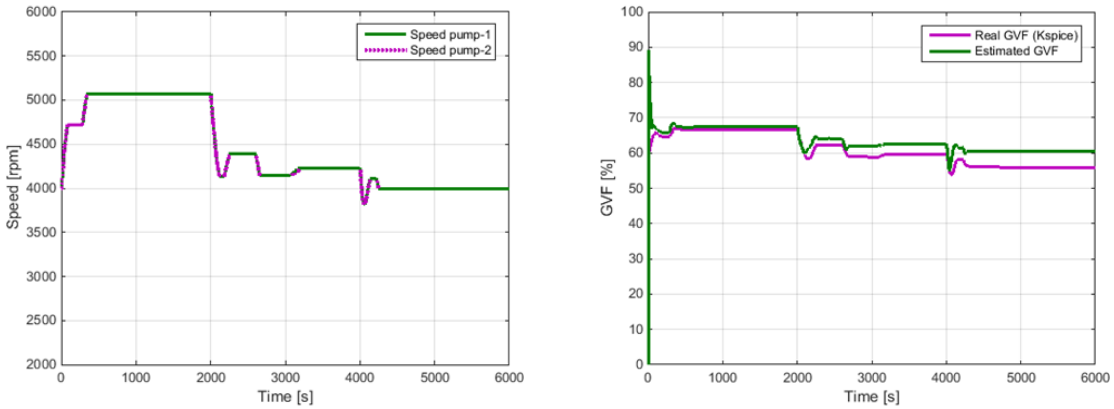

(a) Pump operational speeds.

(b) GVF estimated.

Figure 3-3: GVF estimation in the presence of load controller and HRS.

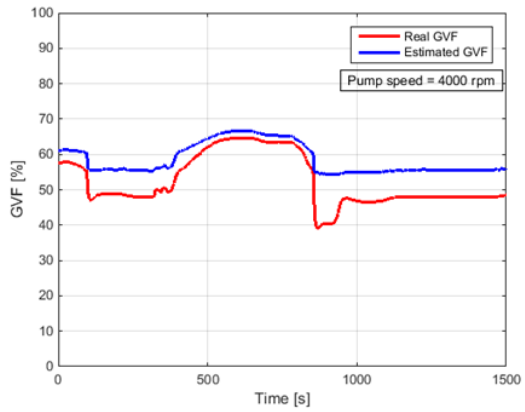

(a) GVF estimation at 4000 rpm pump speed.

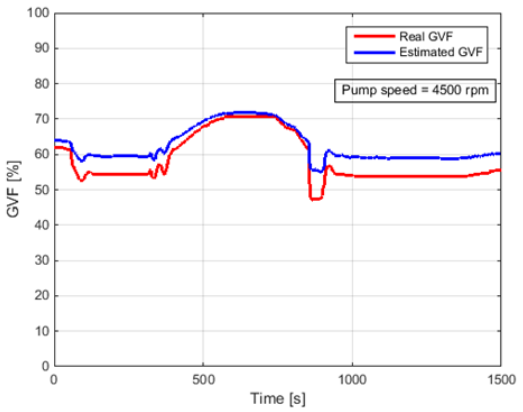

(b) GVF estimation at 4500 rpm pump speed.

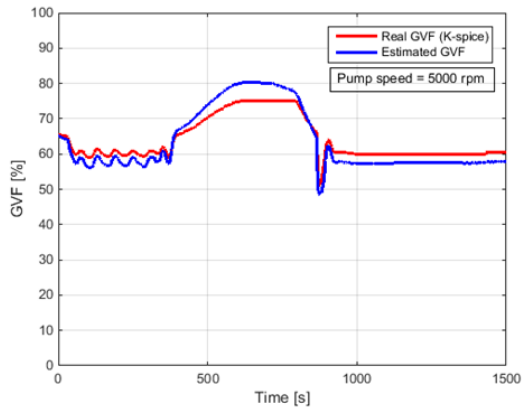

(c) GVF estimation at 5000 rpm pump speed.

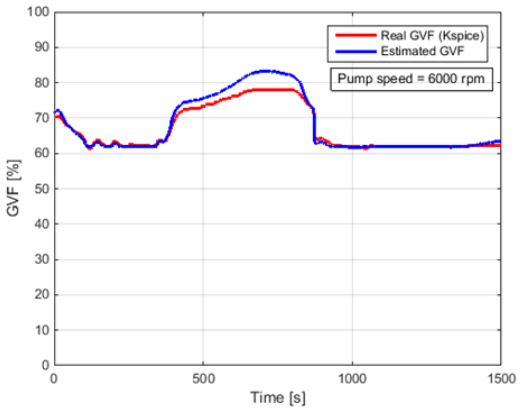

(d) GVF estimation at 6000 rpm pump speed.

Figure 3-4: GVF estimation at different pump speeds

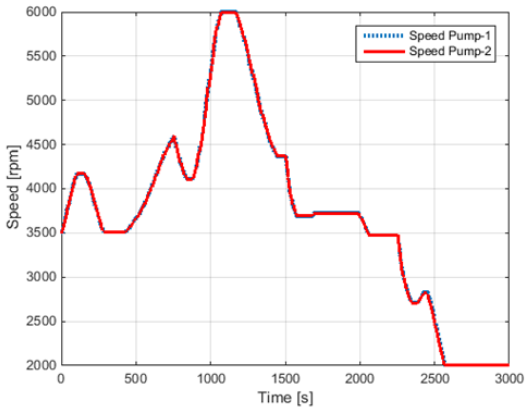

(a) Varying pump speeds.

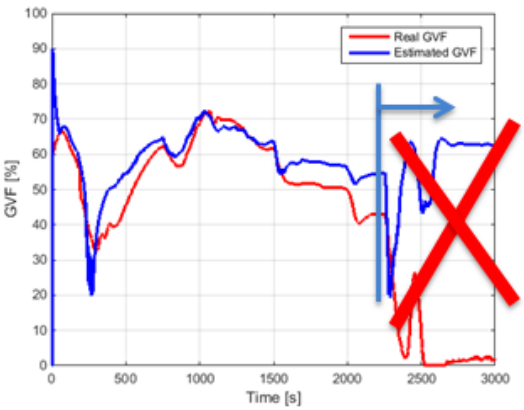

(b) Corresponding GVF estimated.

Figure 3-5: GVF estimation by varying pump speeds

In Fig. 3-3 the GVF estimation algorithm is tested while slowly varying the average and gas valves opening of the reservoir (refer Fig. 2-2). By varying these valve openings, the GVF composition at the inlet of the pump varies. In Fig. 3-3b the estimated GVF is compared with real GVF obtained from Kspice. While the estimation is a close match to the actual value for higher GVF range (65% and above), the estimation is poor for GVFs lower than this range.

For further investigation, the GVF estimation algorithm is tested at different pumps' speeds. While testing the same, the recirculation valve is kept at a constant opening of 20%.

From Fig. 3-4 and Fig. 3-5 it can be observed that the estimation is indeed good for higher GVFs but not necessarily for GVFs lower than 65%.

Possible reasons for poor GVF estimation are listed as:

- **Less data points of pump maps for lower GVFs**
  We only have operating points in the pump maps for 30% and 0% GVF, whereas the operating points are more dense for higher GVF's. For higher GVFs of 50%, 60%, 70%, 80% and 90% operating points exist.
- **Surfaces for different GVF values cross**
  As it can be observed from Fig. 3-6, the GVF surfaces intersect and cross over each other for lower speeds. Which implies, there exist several combinations of GVF and volume flow for the same power, speed and differential pressure. In other words, the function is many to one.

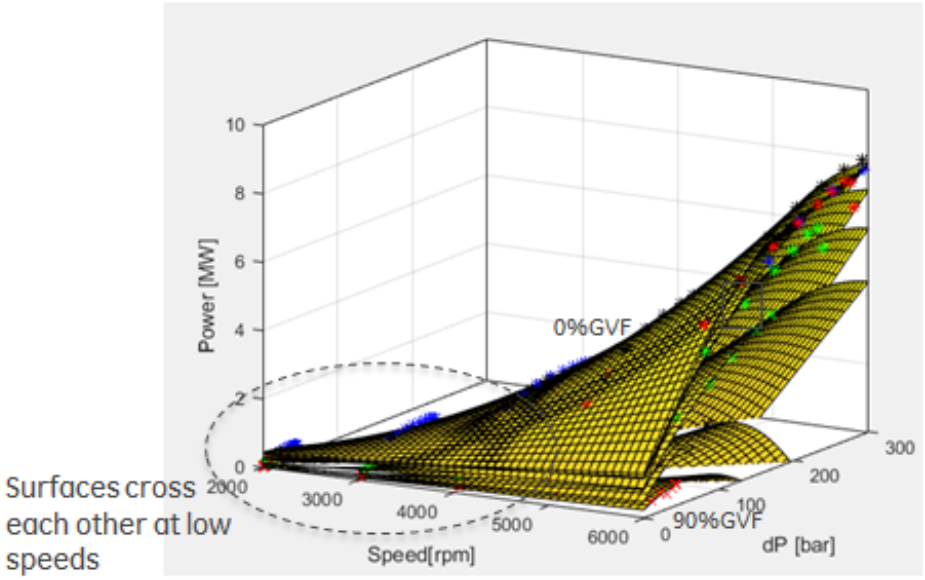

Figure 3-6: Cross over of GVF surfaces for lower speeds.

In order to further improve the GVF estimation, it is mandatory to have more dense and precise pump maps. At this point of time, it is not advised to rely on the GVF estimation algorithm for monitoring GVF at the inlet of the pumps. In the forthcoming simulations, pump inlet GVFs are values taken directly from K-Spice.

3-2 Reservoir volume flow estimation

To estimate volume flow from the reservoir, use is made of available sensor information at the inlet of the boosting station. As shown in Fig. 3-7, a valve is present at the boosting station inlet. The pressure at the inlet ($P_{in_{valve}}$) and outlet ($P_{out_{valve}}$) is known (refer 1-1).

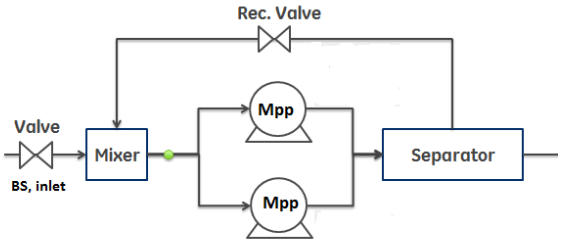

Figure 3-7: Schematic overview of the boosting station.

Therefore the estimation problem translates to relating estimated reservoir volume flow at boosting station inlet ($VF_{res_{est}}$) in terms of the known quantities:

$$VF_{res_{est}} = f(P_{in_{valve}}, P_{out_{valve}}). \tag{3-4}$$

According to the Bernoulli Model [23]:

$$Q = Kv \cdot \sqrt{\frac{\Delta P \cdot 1000}{\rho}}, \tag{3-5}$$

where Q is flow rate through the valve in [m^3/h], ΔP is pressure difference across the valve, Kv is the flow coefficient of the valve and ρ is the liquid density in [kg/m^3]. 3-5 is valid only for pure liquid flow and not a multiphase flow. The density plots assuming reservoir flow is pure liquid (ρ_{liq}) vs the actual reservoir flow density (ρ_{res}) are shown in Fig. 3-5a.

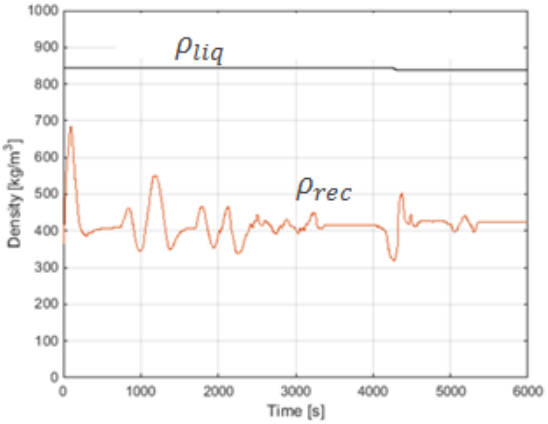

Figure 3-8: Density comparison: pure liquid and actual density.

From Fig. 3-5a it can be observed that $\rho_{liq} > \rho_{res}$. As a result, if 3-5 is applied using ρ_{liq} instead of ρ_{res} the subsequent volume flow obtained will be lesser. To avoid overestimation, use is made of pure liquid density ρ_{liq} (840 kg/m^3) to estimate reservoir volume flow. Using the Bernoulli model from 3-5 we have:

$$VF_{res_{est}} = Kv \cdot \sqrt{\frac{(P_{in_{valve}} - P_{out_{valve}}) \cdot 1000}{\rho_{liq}}}. \tag{3-6}$$

In the simulation below, using 3-6 the reservoir volume flow in [m^3/h] is estimated. The result is compared in Fig. 3-9 with the actual reservoir volume flow obtained from K-Spice.

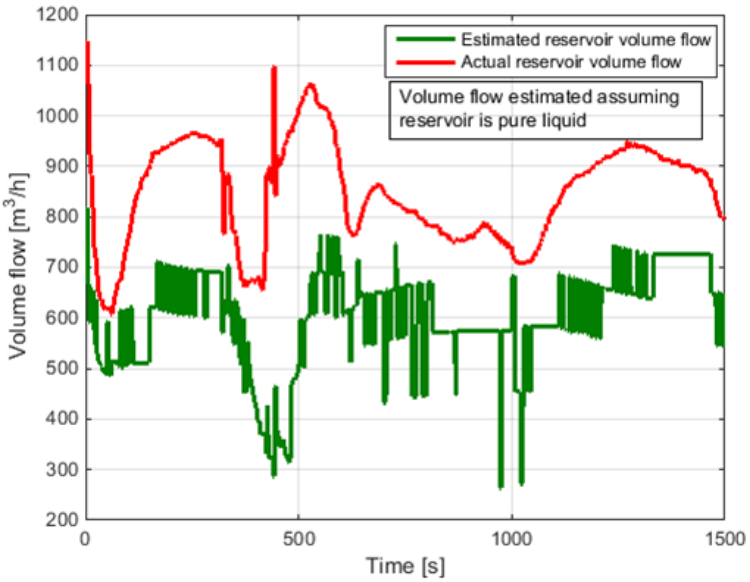

Figure 3-9: Estimation of reservoir volume flow.

From Fig. 3-9 it is observed that the estimated volume flow is lesser than the actual volume flow. Estimating lesser flow than the actual is useful as explained in the next chapter. Also, the result is in accordance with the fact that pure liquid has a lesser volume flow than a flow composed of liquid and gas (actual reservoir flow).

Chapter 4

Controller Synthesis

In this chapter, various controllers pertaining to the general safety and reliable operation of the boosting station are designed. Addressing the identified control objectives, the different controllers synthesized are: Master controller, Load sharing controller, Minimum flow and GVF controller and an anti-slug controller for riser slugging.

The controllers are synthesized in MATLAB/Simulink. These controllers receive the sensor measurements pertaining to the process from the integrated K-Spice/LedaFlow model via the OPC link (refer Fig. 2-6). Likewise, the actuation commands are sent back from the controllers to the integrated model through the bidirectional OPC link.

4-1 Control architecture

The control architecture shown in Fig. 4-1 is adopted for the operation of the controllers designed for boosting station. The control architecture of the boosting station is composed of cascaded controllers namely Master controller, Load sharing controller, Minimum flow and GVF controller.

The outputs of the Master and Load sharing controllers are sent to the load controller. In the load controller, static and dynamic limiters are present which limit the outputs of the Master and Load sharing controllers before sending it to the boosting station. The load controller typically alters the state of the pumps.

The Minimum flow and GVF controllers are used to control the recycle valve opening. The anti-slug controller for riser slugging is not explicitly shown in Fig. 4-1. The various controllers are elaborated and detailed in the forthcoming sections.

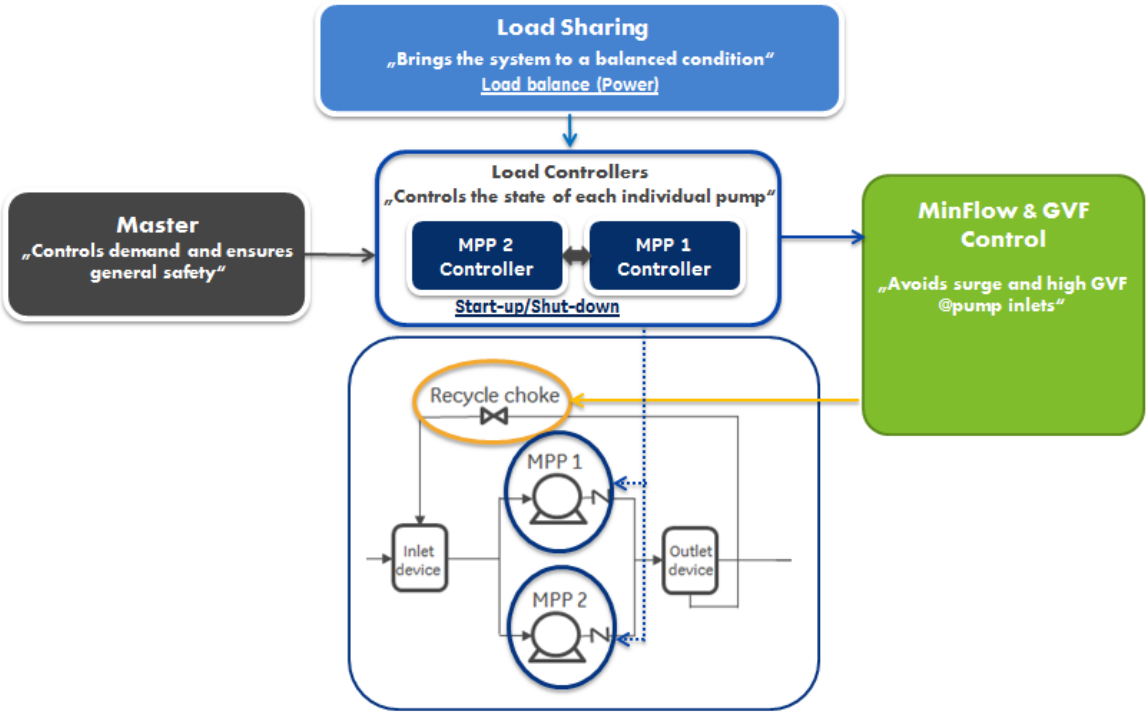

Figure 4-1: Overview of the control architecture.

4-2 Master controller

The master controller controls demand and ensures general safety of the boosting station. Demand is defined by the customer end. The process demand may be in terms of:

- Desired discharge pressure at each of the pump outlets.
- Desired suction pressure at each of the pump inlets.
- Desired mass flow of the reservoir fluid at mixer outlet.
- Torque control.

The customer defines the set-point of the process demand variable. Using the sensor measurement, we feedback the actual measured value of the process demand variable. As shown in Fig. 4-2 the master controller is implemented by using a PID controller for each of the pumps. d may be one of the aforementioned process demand variables. The output of the PID controller is used to alter the speed of the pumps. The PID controller continuously varies the speed of the pumps till the set-point is reached.

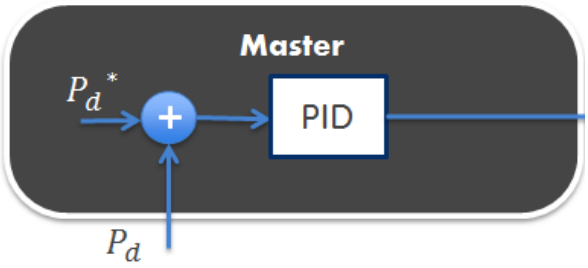

Figure 4-2: The Master Controller.

The actuator for the master controller is the pump speed. The output of the master controller is fed into the Load Controllers (refer Fig. 4-3). In the load controller static and dynamic limiters are applied on the pump speed. After the limiters, the load control output is fed to the multiphase pumps thereby altering the state of the MPPs.

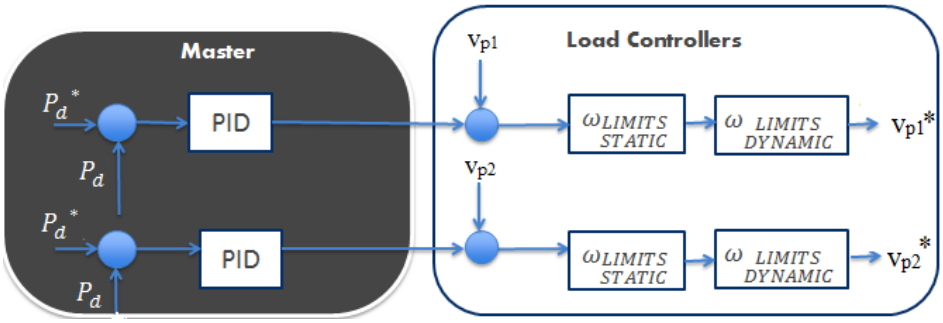

Figure 4-3: Master controller and load controllers.

In the load controller, the static limitation is based on the fact that the MPPs operate only between 2000 and 6000 rpm. Therefore the pump speed is clipped so as to remain in between these boundaries.

The dynamic limiters are based on:

- Increase/Decrease in the rate of speed: The pump takes 60 seconds to increase it's speed from 0% to 100%. The pump also takes 300 seconds to stop completely (100% to 0%). Based on this, the rate at which the pump speed can increase or decrease is limited in the Simulink model by using the dynamic saturation block. The rate at which the pump speed can rise is limited at 10.47 rad/s and the rate at which the pump speed can decrease is limited at -5.23 rad/s.
- Resolution: Internally, the pump considers only counts (25000 counts = 100%). The pump has a finite resolution of 1% implying that if the change in control signal is less than 1% (250 counts), there is no change in the pump speed. The current pump used has a resolution of 6.28 rad/s. Pump speed resolution is implemented in Simulink by introducing a small delay between successive input signals (refer Fig. 4-4). When the difference is greater than the pump speed resolution, the latest signal is passed. Else, the speed remains unchanged.

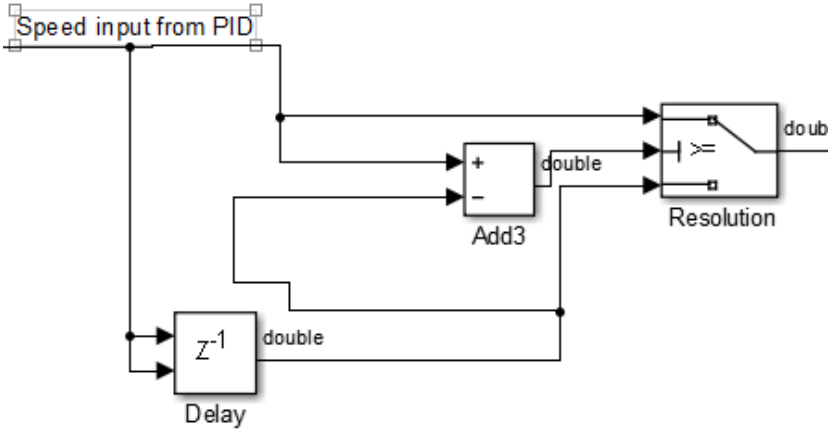

Figure 4-4: Threshold block implemented in Simulink.

- Additionally, a speed limiter is used to limit the speed as a function of GVF or differential pressure based on the operating envelope of the pump (refer Fig. 4-5 and Fig. 4-6. Operators with pump operational experience fix this envelope.
  Though the MPP speed can lie between 2000 and 6000 rpm, there are further limitations on the speed range in which the pump can operate based on the curent GVF at the pump inlet or the differential pressure across the pump. In Fig. 4-5 the operating envelope based on current GVF is given. Since it is tough to obtain measurements on pump inlet GVF as mentioned earlier, the operating envelope based on the differential pressure across the pumps is also defined (refer 4-6). The speed limiter based on the operating envelope is currently implemented in Simulink by two look-up tables and a dynamic saturation block, although s functions can also be used.

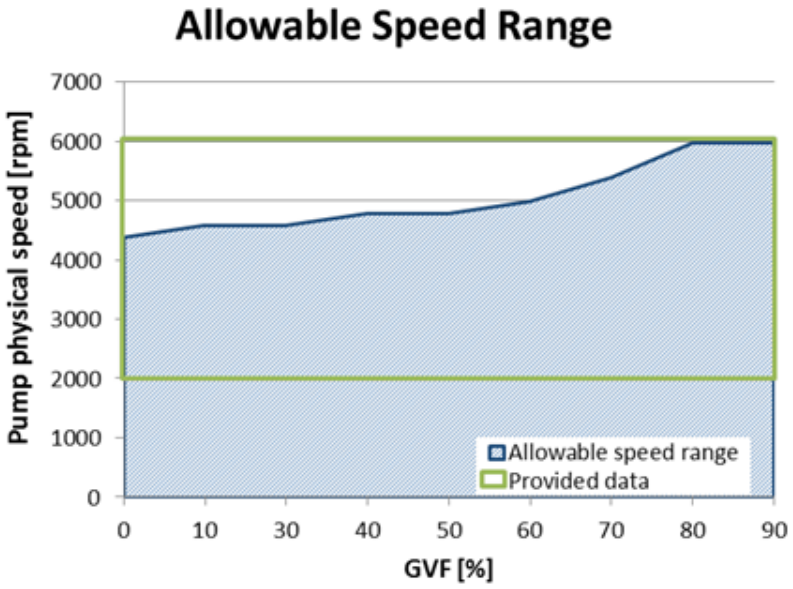

Figure 4-5: Pump physical speeds envelope based on GVF.

GVF	Speed_min	Speed_max	Speed_band	dP (tested)	dP (from map)
[%]	[rpm]	[rpm]	[rpm]	[bar]	[bar]
0	0	4400	4400	170	220
10	0	4600	4600	170	205
30	0	4600	4600	170	190
40	0	4800	4800	160	180
50	0	4800	4800	130	170
60	0	5000	5000	130	150
70	0	5400	5400	110	130
80	0	6000	6000	100	90
90	0	6000	6000	100	50

Figure 4-6: Pump physical speeds envelope based on differential pressure.

The working of the master controller is tested in the co-simulation environment. The process demand variable was discharge pressure at pump outlet. 65 bar was set as desired discharge pressure at each of the pump outlets. The simulation results of discharge pressures, pump speeds and respective power consumed are shown in Fig. 4-7.

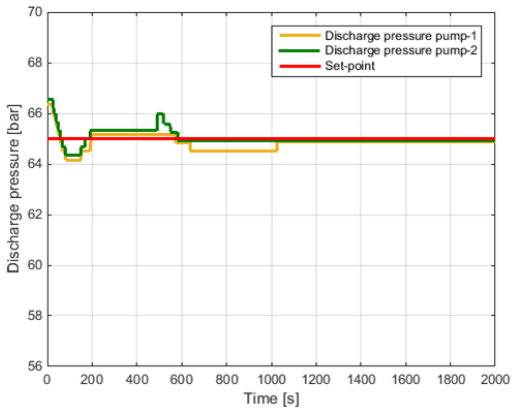

(a) Discharge pressure at pump outlets.

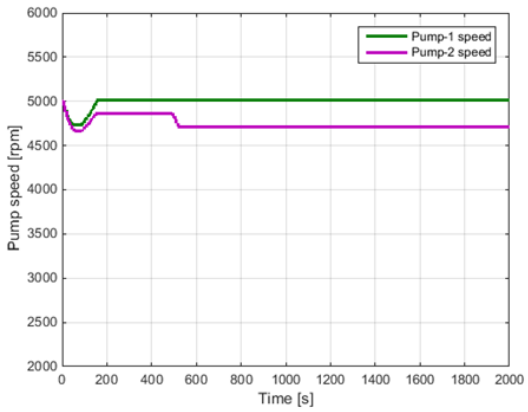

(b) Pump operational speeds.

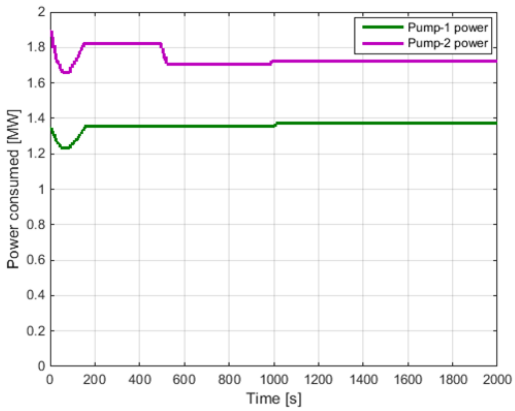

(c) Power consumed by the pumps.

Figure 4-7: Process demand controls: Discharge pressure.

It is observed in Fig. 4-7a that the discharge pressure set-point has been attained by the master controller. However, from Fig. 4-7c it can be observed that the power consumed by the pumps is not equal. One pump effectively consumes more power than the other. That means the load (reservoir flow) is not equally distributed across the pumps. In 1-4 load distribution across the MPPs was identified as a control objective. Therefore, a load sharing controller to balance the load is to be introduced.

4-3 Load sharing controller

The boosting station is composed of two MPPs (refer Fig. 1-3). The reservoir flow (load) enters each of the pumps which subsequently boost/add energy to the multiphase stream. In the real scenario, it is likely that the load on one pump is greater than the other (refer reasons for asymmetric split of reservoir flow listed in 1-3). As the MPPs are going to operate parallelly, it is required to ensure that the load is balanced between the pumps.

The goal of load sharing controller is to balance the load. Load on each of the pumps is reflected in the form of power consumed by the pumps. The load sharing controllers consist of a PID controller for each of the MPPs. The set-point of each of these PIDs is the average of the instantaneous power consumed by the pumps. The set-point is chosen in such a way that even if the initial power consumed by the pumps are different, over time they will converge to a common power consumption. For feedback input for each of the PIDs, the current power consumed by the pumps is used.

The actuator for the load sharing controller is also pump speed as in the case of the master controller. For this reason the control loops of load sharing and master controller are coupled together. Since the control inputs may counteract each other, the PID gains of load sharing controller are made more aggressive than the others. As it can be seen in Fig. 4-8, the control inputs of master and load sharing controller are coupled in the load controller. Static and dynamic limiters are once again applied on the pump speeds before being sent to the MPPs.

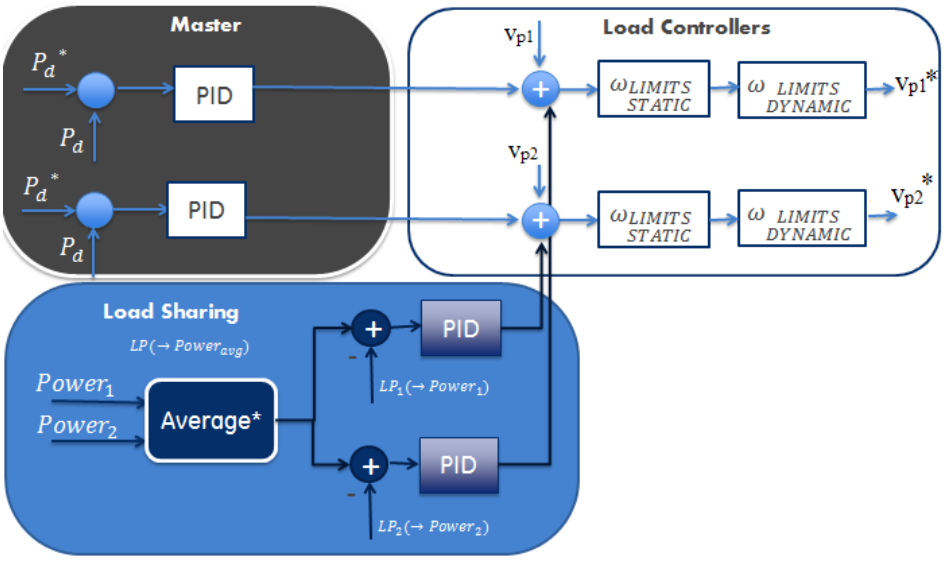

Figure 4-8: Load sharing controller coupled with the master and load controller.

The load sharing controller is tested using the simulation environment and the results are presented in Fig. 4-9. To be noted is that the load sharing controller and the master controller operate together.

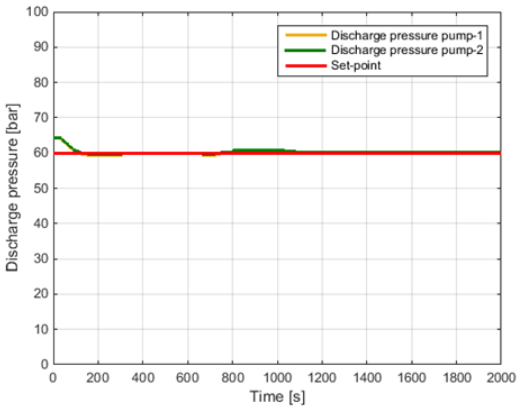

(a) Discharge pressure at pump outlets.

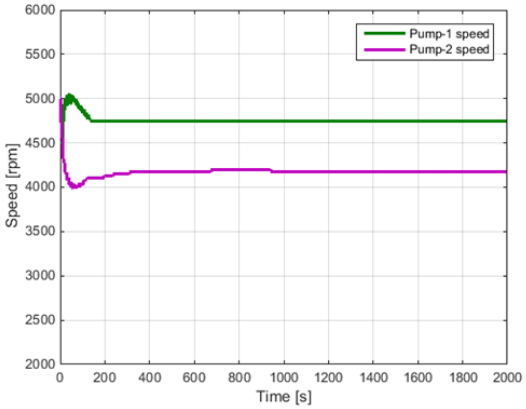

(b) Pump operational speeds.

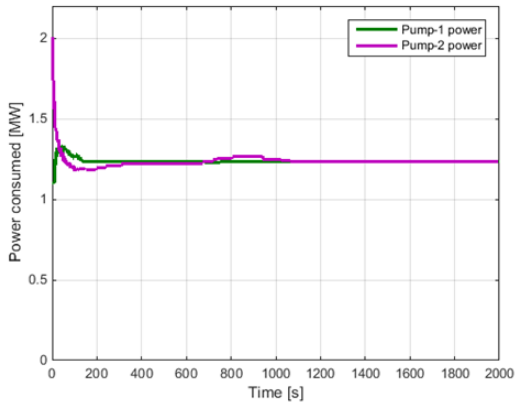

(c) Power consumed by the pumps.

Figure 4-9: Load sharing and master controls

In Fig. 4-9a it can be observed that the discharge pressure at the pump outlets is controlled to the desired set-point. Also from Fig. 4-9c it is evident that the power consumed by each pump is equal over time. Therefore, it is inferred that the load is equally distributed. Notice that although the pump speeds (refer Fig. 4-9b) are not equal, the power consumed is equal. This is possible as from the pump maps one can observe that the data points corresponding to different operating speeds may still have the same power consumption.

In Fig. 4-10 results obtained by testing the load sharing and master controller again are presented. Differently from the previous scenario, desired mass flow at mixer outlet is chosen as the demand process variable. Moreover, for the master controller the desired mass flow at mixer outlet has a time varying set-point.

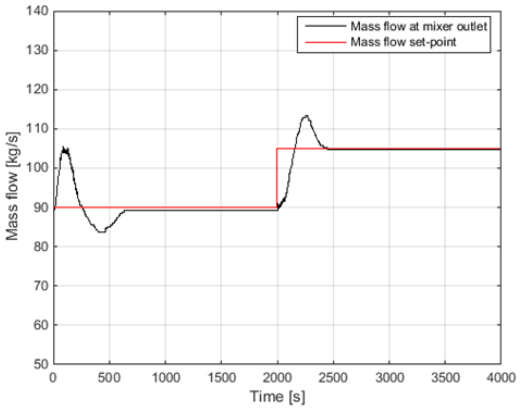

(a) Mass flow at mixer outlet.

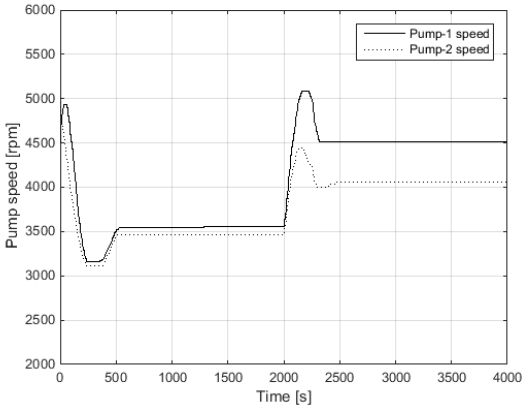

(b) Pump operational speeds.

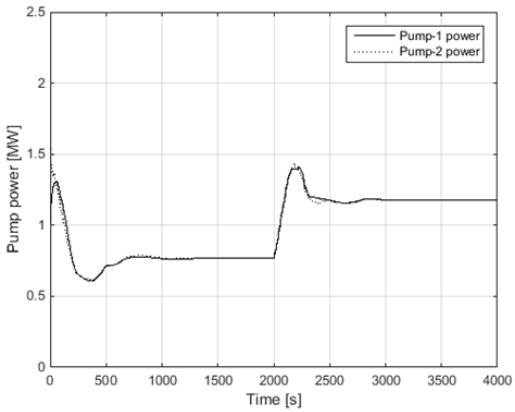

(c) Power consumed by the pumps.

Figure 4-10: Mass flow controls.

It can observed from Fig. 4-10a that the mass flow tracks the corresponding desired set-point. Also, the power consumed by the pumps is equal (refer Fig. 4-10c), therfore the load sharing controller has balanced the loads between the MPPs.

4-4 Minimum flow and GVF control

For the safety of the multiphase pumps, it is essential to ensure that minimum flow into the pump and maximal GVF at the pump inlet are not violated.

Minimum flow control: The multiphase pumps present in the boosting station require a constant volume flow into them to avoid surge. If the flow from reservoirs is not sufficient to avoid surging, the recirculation valve (refer Fig. 1-3) is used to recirculate an extra amount of liquid back to the mixer from separator. The minimum flow controller calculates the required recirculation valve opening so as to recirculate the extra required flow to avoid surge.

GVF control: The role of the GVF controller is to ensure that the GVF at the inlet of the pumps is always under the prescribed limit.

In this chapter, based on sensor and instrumentation availability, three strategies are presented to ensure the objectives of minimum flow control and GVF control are achieved. The three strategies are: Baseline strategy, High robustness strategy (HRS) and High performance strategy (HPS). The subsequent production obtained is compared.

4-4-1 Baseline strategy

In the baseline strategy, the recirculation valve has a constant opening, independent of the current operation conditions [24]. The constant position is chosen in such a way that the gas volume fraction (GVF) at the pump inlet is under the prescribed limit even for the longest duration of reservoir slugs, while at the same time assuring minimum flow into the pumps. The baseline strategy requires only basic sensor measurements. Consequently, it is easy to implement. However, in the long run we pay a penalty in the efficient operation of the pumps as we keep recirculating large amounts of liquid flow back to the pump.

4-4-2 High robustness strategy

The High Robustness Strategy (HRS) is a fallback strategy based on the static pump maps. The HRS requires only intermediate number of sensors and it can be used even in the absence of an MPFM. The HRS assures minimum flow into the pumps for the worst case GVF (i.e minimum flow control independent of the current GVF). Therefore, this strategy can be used even when no GVF measurements are available. As demonstrated in the later sections, the efficiency gain on pump operation is more than that of the baseline strategy.

For the HRS strategy, it is important to know the minimum volume flow required by each of the pumps. For finding the minimum flow, use is made of the pump maps. Two different minimum flow determination methods based on pump maps are first proposed and then compared.

4-4-2-1 Minimum flow line

The different operating points of the pump maps are arranged in an increasing order of the GVFs. That is, these data points are arranged from 0 to 90% GVF. A MATLAB plot is made for these data points with differential pressure/speed (dp/speed) on the x axis and volume flow on the y axis. The result is as shown in Fig. 4-11

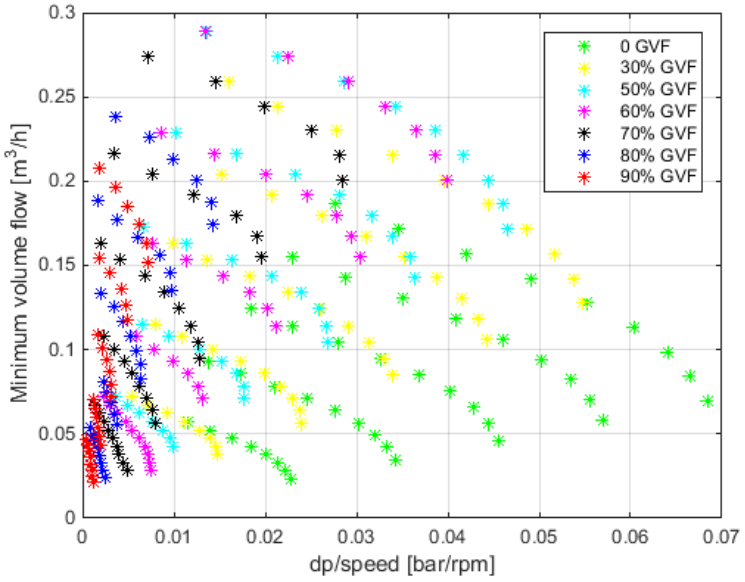

Figure 4-11: Data points of the pump maps.

For each and every point on x axis (differential pressure/speed), minimum flow into the pumps independent of GVF (i.e it should satisfy minimum flow requirements for 0% and also 90% GVF) is to be ensured. Using `ginput` command of MATLAB 6 points are obtained (x, y data points from Fig. 4-11). A piecewise affine function is fit to pass through these points as shown in Fig. 4-12.

The piecewise affine function ensures that for every point on the x axis, minimum flow (min-flow) is ensured independent of the current operating GVF. The piecewise affine function with x axis as differential pressure/speed in [bar/rpm] and y axis as minimum flow in [m^3/h] is shown in Table 4-1.

Table 4-1: The minimum flow line.

Function	Domain of x
$y = 8.6445 \cdot 10^4 x$	$(0 \quad 0.0049)$
$y = 5.7502 \cdot 10^4 x + 141.2053$	$(0.0049 \quad 0.0071)$
$y = 1.0988 \cdot 10^4 x + 472.2759$	$(0.0071 \quad 0.0143)$
$y = 6.5930 \cdot 10^3 x + 534.4992$	$(0.0143 \quad 0.0285)$
$y = 722.9651$	$(0.0285 \quad 0.07)$

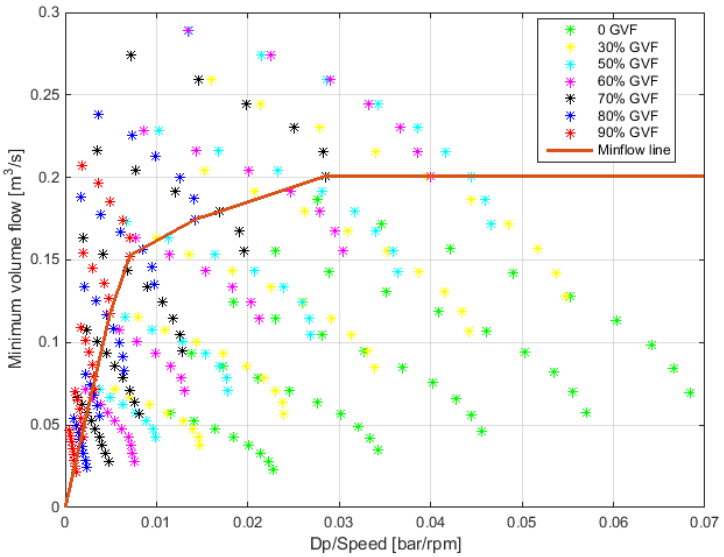

Figure 4-12: Minimum flow line.

The minflow line in Fig. 4-12 can be implemented in Simulink as a lookup table. Using this line, given differential pressure and speed of the pump we can find the minimum flow required by the pump (independent of GVF) to prevent surge.

4-4-2-2 Minflow surface

Alternatively, a 3-D plot is made using all the operating points by plotting differential pressure on x axis, speed on y and volume flow on z axis. Using the MATLAB command `fit`, a surface is fit to these points. The intercept is changed in such a way that the surface lies below all the points. The model type chosen is `poly21` therefore we have a polynomial surface of degree 2 in x and degree 1 in y. In our case, the x corresponds to differential pressure and y corresponds to pump speed. The linear model `poly21` is given by:

$$Minflow(dp, v_p) = 0.95 \cdot (p_{00} + p_{10}dP + p_{01}v_p + p_{20}dP^2 + p_{11}dPv_p), \tag{4-1}$$

with the polynomial coefficients:

$$p_{00} = -32.69 \quad p_{10} = -2.444 \quad p_{01} = 0.07887 \quad p_{20} = -0.009837 \quad p_{11} = 0.0009795. \tag{4-2}$$

In comparison to the 1-D lookup table of the minflow line, the minflow surface in Fig. 4-13 ensures smoother and less conservative operation of the recirculation valve.

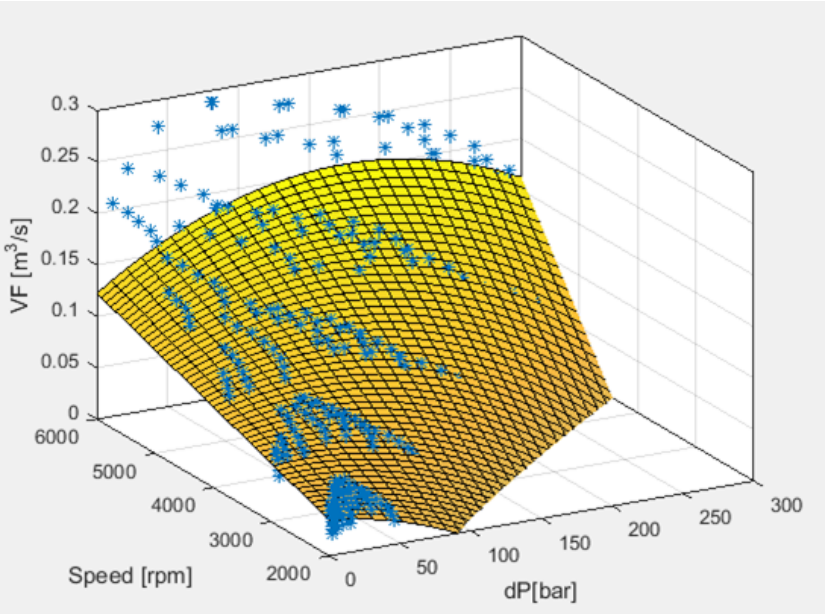

Figure 4-13: Minimum flow surface.

4-4-2-3 The HRS algorithm using bernoulli model

Once the minimum flow required by the pumps to avoid surge is found, the recirculation valve needs to be opened if sufficient reservoir flow is not present.

The recirculation valve opening using HRS algorithm can be calculated in 4 steps:

1. The minimum volume flow required by each of the pumps is calculated using either the minflow line or minflow surface.

$$VF_{1_{minflow}} = HRS_{line/surface}(P_{in_1}, P_{out_1}, v_{p_1}) \tag{4-3}$$
$$VF_{2_{minflow}} = HRS_{line/surface}(P_{in_2}, P_{out_2}, v_{p_2}) \tag{4-4}$$

   where $VF_{1_{minflow}}$, $VF_{2_{minflow}}$ are minflow in [m^3/s] required by pump 1 and pump 2 respectively, P_{in_1}, P_{in_2} are suction pressures in [bar], P_{out_1}, P_{out_2} are discharge pressures in [bar], v_{p_1}, v_{p_2} are speeds in [rpm] and the subscript 1 and 2 represent pump 1 and pump 2 respectively.

   The suction, discharge pressures and pump speeds are available measurements. The difference between discharge and suction pressure is differential pressure. Since differential pressures and pump speeds are known, use is made of the minflow line or surface to find minimum volume flow required by the pumps in 4-4.

2. Overall minimum flow required by both the pumps is defined taking uncertainty like splitting etc. into account. The worst case minimum flow required is given by:

$$VF_{worstcase,req} = 1.05 \cdot (VF_{1_{minflow}} + VF_{2_{minflow}}) \tag{4-5}$$

3. The volume flow from the reservoir as explained in 3-2 is estimated. The estimated reservoir volume flow at boosting station inlet ($VF_{res_{est}}$) is expressed in terms of:

$$VF_{res_{est}} = f(P_{in_{valve}}, P_{out_{valve}}). \tag{4-6}$$

4. From Fig. 4-14, it is observed that at the mixer, the two flows from reservoir and recirculation valve merge. Therefore, the actual volume flow required by both the pumps together is given by:

$$VF_{req} = VF_{worstcase,req} - VF_{res_{est}}. \tag{4-7}$$

After subtracting $VF_{worstcase,req}$ (calculated in step 2) from $VF_{res_{est}}$ (calculated in step 3) we are left with VF_{req} in [m^3/s]. This actual volume flow VF_{req} required by both the pumps should be supplied by the recirculation flow. As a result, it is required to calculate the recirculation valve opening so as to guarantee VF_{req} in the form of recirculation flow.

Based on available sensor information, the recirculation valve opening α is expressed in terms of:

$$\alpha = min(0.05, f(VF_{req}, dP_{rec}, \rho_{rec})), \tag{4-8}$$

where dP_{rec} is the pressure drop across the recirclaton valve in [m], ρ_{rec} is density of the recirculation mixture in [kg/m^3]. In 4-8 the constant 0.05 occurs to ensure a minimum of 5% opening of the recirculation valve to prevent hydrate formation.

The separator ensures the recirculation flow consists of only pure liquid. Therefore, it is possible to apply the bernoulli model in 3-5 to find the valve opening α. Applying the bernoulli model, we express the required volume flow VF_{req} as:

$$VF_{req} = Kv_{rec} \cdot \sqrt{\frac{dP_{rec} \cdot 1000}{\rho_{rec}}}. \tag{4-9}$$

In 4-9 the valve flow coefficient can be related to valve opening α. For the recirculation valve, 100% opening corresponds to a Kv of 259.5. Therefore, 4-9 can be rewritten to calculate α by the following equation:

$$\alpha = \frac{VF_{req}}{Kv_{rec}} \cdot \sqrt{\frac{\rho_{rec}}{dP_{rec} \cdot 1000}} \tag{4-10}$$

From 4-8 it is evident that the subsequent recirculation valve opening is minimum of 0.05 (5%) or the opening calculated by 4-10.

The final recirculation valve opening obtained by the HRS algorithm using the Bernoulli model is given by:

$$\alpha = min\left(0.05, \frac{VF_{req}}{Kv_{rec}} \cdot \sqrt{\frac{\rho_{rec}}{dP_{rec} \cdot 1000}} \right). \tag{4-11}$$

The HRS algorithm using Bernoulli model consists of 4 steps as indicated above. The point of action of each and every step in the subsea boosting station is summarized in Fig. 4-14.

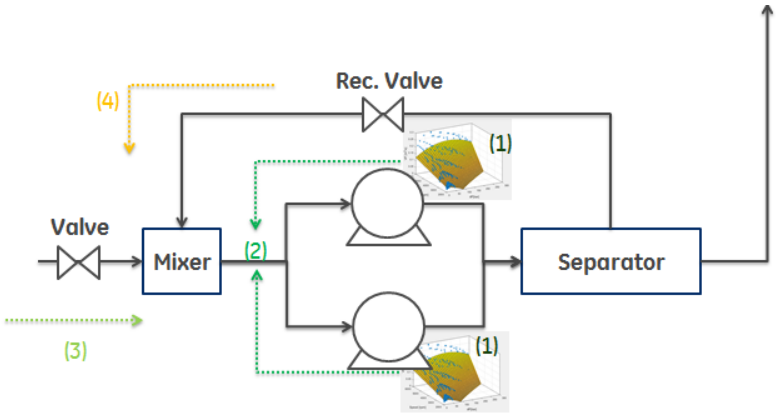

Figure 4-14: Valve opening calculation using HRS in 4 steps.

The HRS algorithm using Bernoulli model (refer 4-4-2-3) is summarized in the flowchart given in Fig. 4-15.

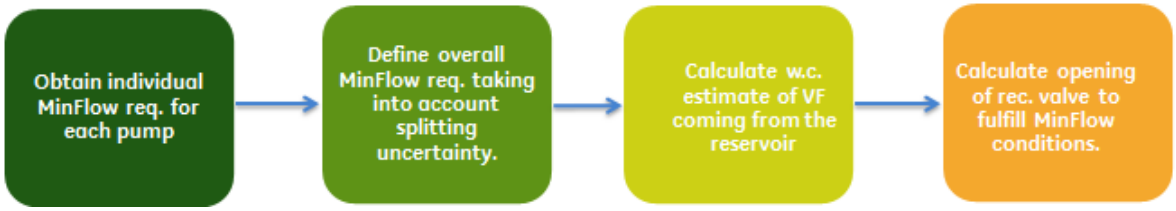

Figure 4-15: Flowchart for the HRS algorithm.

Results obtained by testing the HRS algorithm using Bernoulli model (refer 4-4-2-3) are presented in Fig. 4-16. For comparison, two sets of simulations are run with same initial conditions using the minflow line and minflow surface respectively for calculating $VF1_{minflow}$ and $VF2_{minflow}$ in step 1 of the HRS algorithm. Also a 2 minute reservoir slug (generation of slugs explained later) was introduced close to the 1000th minute.

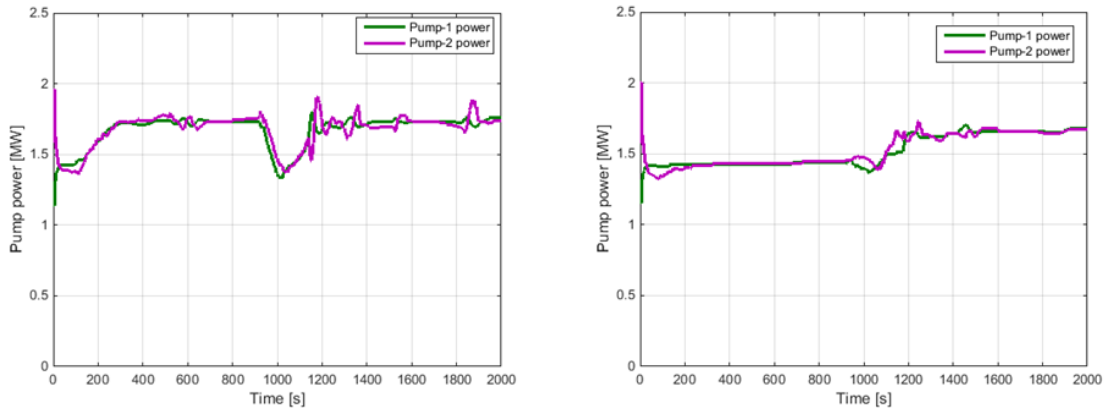

(a) Power consumed using minflow line.

(b) Power consumed using minflow surface.

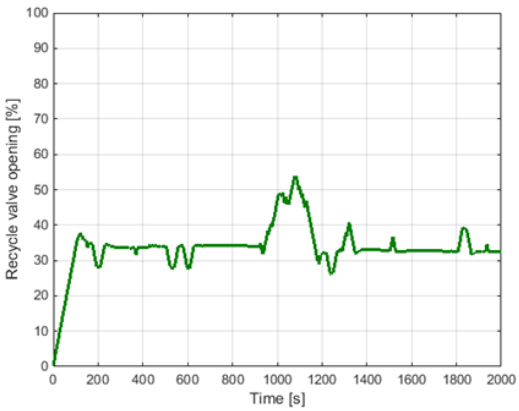

(c) Valve opening using minflow line.

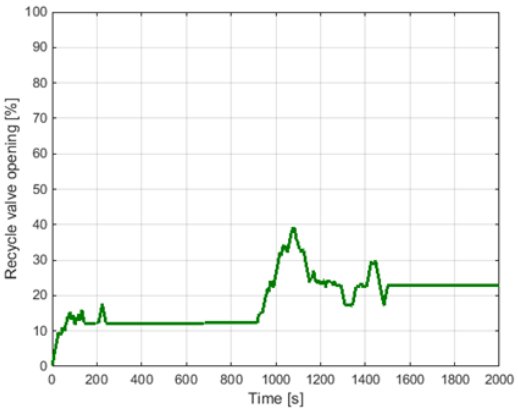

(d) Valve opening using minflow surface.

Figure 4-16: Minflow line vs surface comparison.

From Fig. 4-16a and Fig. 4-16b it can be observed that pumps consume lesser power with the minflow surface. Also from Fig. 4-16c, Fig. 4-16d it is evident that valve opening is less by around 20% when using the minflow surface. These observations re-emphasize that the minflow surface ensures smoother and less conservative operation of the recirculation valve. Therefore, in future simulations of the HRS algorithm the minflow surface will only be used.

4-4-2-4 The HRS algorithm using homogeneous equilibrium models (HEM)

The HRS algorithm using Bernoulli model (refer 4-4-2-3) assumes that the fluid in the recirculation loop consists of pure liquid. Strictly speaking, due to the relatively high pressure drop across the recirculation valve, it so happens that some of the pure liquid gets converted to gaseous phase. This phenomenon is also known as flashing. For this case, in order to calculate the recirculation valve opening the following factors must be considered:

- The valve model should be accountable for multiphase flow.
- The model should be applicable to flashing.

The model suitable for our scenario is the Homogeneous Equilibrium Models (HEM). It has three variants namely:

- Two-phase Multipliers
- Omega Method
- Homogeneous Direct Integration (HDI)

Although all three variants can be used, for convenience sake we make use of the Homogeneous Direct Integration (HDI) method. The HDI method is based on numerical integration of mass flux integral with linear interpolated grid formed based on input and output pressures [25].

The recirculation valve opening for HRS algorithm using HEM can be calculated in the following steps:

1. The minimum volume flow required by each of the pumps is calculated using the minflow surface.

$$VF_{1_{minflow}} = HRS_{surface}(P_{in_1}, P_{out_1}, v_{p_1}) \tag{4-12}$$

$$VF_{2_{minflow}} = HRS_{surface}(P_{in_2}, P_{out_2}, v_{p_2}) \tag{4-13}$$

2. Overall minimum flow required by both the pumps is defined taking uncertainty like splitting etc. into account. The worst case minimum flow required is given by:

$$VF_{worstcase,req} = 1.05 \cdot (VF_{1_{minflow}} + VF_{2_{minflow}}) \tag{4-14}$$

3. Volume flow from the reservoir as explained in 3-2 is estimated. The estimated reservoir volume flow at boosting station inlet ($VF_{res_{est}}$) is expressed in terms of:

$$VF_{res_{est}} = f(P_{in_{valve}}, P_{out_{valve}}). \tag{4-15}$$

4. From Fig. 4-14, it is observed that at the mixer, the two flows from reservoir and recirculation valve merge. Therefore, the actual mass flow required by both the pumps together is given by:

$$\dot{m}_{req} = \rho_{p_{in}} \cdot VF_{worstcase,req} - \rho_{res} \cdot VF_{res_{est}}, \tag{4-16}$$

where $\rho_{p_{in}}$ is density at pump inlet in [kg/m^3] and ρ_{res} is reservoir density in [kg/m^3].

5. Calculate the theoretical mass flux (mass/time·area) through an isentropic nozzle. The expression for mass flux G_o is given by:

$$G_o = \rho_n \left(-2 \int_{P_0}^{P_n} \frac{dP}{\rho} \right)^{1/2}, \tag{4-17}$$

where P_0 is pressure in [bar] at the entrance to the valve, P_n is pressure in [bar] at the valve outlet, ρ is fluid density in [kg/m^3] at pressure P and ρ_n is the fluid density at pressure P_n.

The HDI method involves generating multiple (P, ρ) data points over an isentropic range of pressures from P_0 to P_n using a thermodynamic-property database for a pure liquid and a flash routine for a multicomponent mixture. This data is used to evaluate the mass flux integral in 4-17, by direct numerical integration. This can be done by a simple quadrature formula as follows:

$$G_o = \rho_n \left(-2 \int_{P_0}^{P_n} \frac{dP}{\rho} \right)^{1/2} \equiv \rho_n \left[-2 \sum_{P_0}^{P_n} \frac{P_{i+1} - P_i}{\bar{\rho}_i} \right]^{1/2}. \tag{4-18}$$

The quadrature formula is implemented by using a PVT table with data of parameters across the valve.

6. The required orifice area for a relief valve is determined by:

$$A = \frac{\dot{m}_{req}}{K_d \cdot G_o}, \tag{4-19}$$

where G_o is calculated in the previous step and K_d is the dimensionless discharge coefficient that accounts for the difference between predicted ideal nozzle mass flux and actual mass flux in the valve. The value of this coefficient is determined by the valve manufacturers from measurements.
The valve opening α is related to the area by:

$$D = \sqrt{\frac{4 \cdot A}{\pi}} \tag{4-20}$$

$$\alpha = \frac{D}{0.1651}, \tag{4-21}$$

where D is the diameter (4.5 inch) of the valve under consideration. The actual valve opening is a minimum of 0.05 (5%) or the one determined by 4-21.

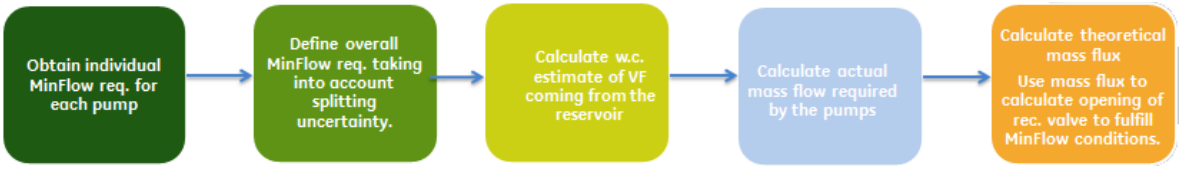

Figure 4-17: Flowchart for the HRS algorithm using HEM.

4-4-2-5 Comparative simulations for bernoulli model vs HEM

In this section, the recycle valve opening is compared with the HRS strategy using Bernoulli model (4-4-2-3) vs HEM (4-4-2-4). A static simulation is first conducted by varying differential pressure across the pumps and across the recirculation valve. In order to aid this simulation, the following assumptions are made:

- Both pumps have the same initial speeds.
- The volume flow from reservoir is exactly measurable. It is kept fixed at 720 m^3/h.
- Since the HEM requires mass flow, it is assumed that measurements of density of the reservoir mixture and density at inlet of the pumps are available.

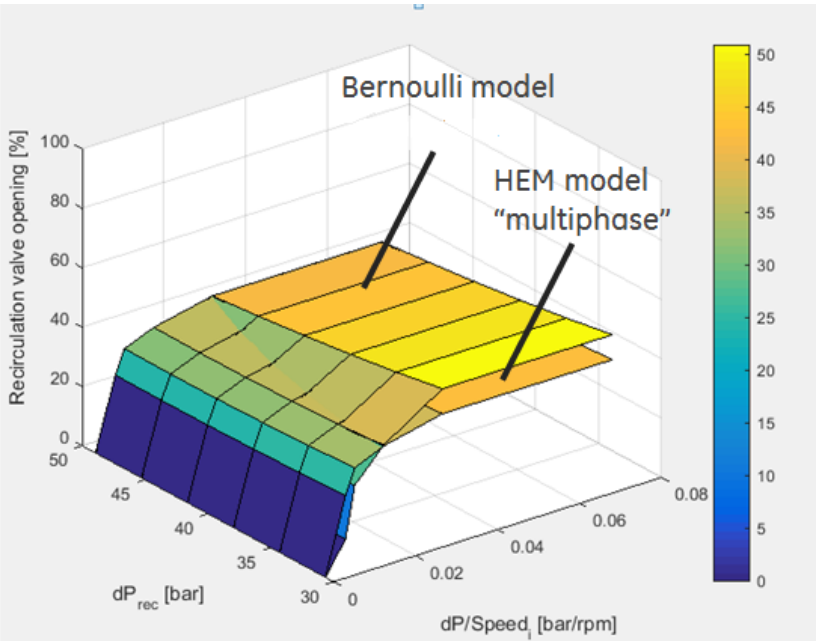

Figure 4-18: Valve opening comparison: Bernoulli vs HEM.

From Fig. 4-18, it can be observed that the valve opening with HEM has a lesser opening than the Bernoulli model. This result is expected, as in the HEM we consider multiphase flow, therefore the volume flow in the recirculation loop is greater. The difference in valve opening between HEM and Bernoulli model is upto 16%.

In order to further test the HRS algorithm with Bernoulli and HEM we perform a dynamic simulation with the K-Spice/LedaFlow integrated model. After bringing the system to a steady state with the same initial speeds for both the pumps, the simulation was started. A 7 minutes reservoir slug was introduced starting at the 300th second.

The reservoir model in K-Spice consists of two wells. An average and gas valve are present for either well as shown in Fig. 2-2. In normal conditions the average valves are opened and the gas valves are closed. This introduces a reservoir mixture flow of GVF around 55% into the boosting station. In order to introduce a slug, the average valves of either well are closed and the gas valves are opened (refer Fig. 4-19). When the gas valves are opened and the average valves are closed, a reservoir flow of 100% GVF (pure gas) is introduced which is a slug.

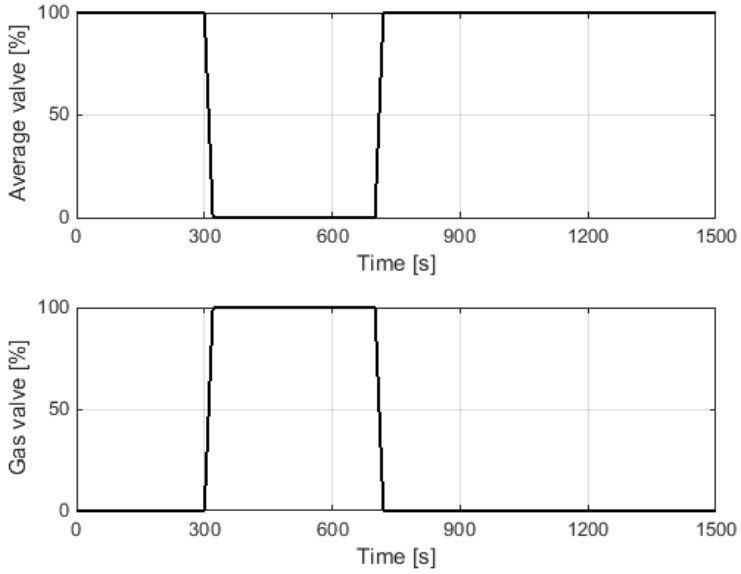

Figure 4-19: Valve openings to introduce 7 minute slug.

The results of the dynamic simulations of HRS for Bernoulli vs HEM are shown in Fig. 4-20 and Fig. 4-21. From Fig. 4-20 and Fig. 4-21 we can say that the HRS strategy performs well with both the Bernoulli and the HEM. The multiphase pumps were able to survive the 7 minute slugs. Also, the GVF was below the hard limitation (80%). Further, from Fig. 4-20 we can observe that the recirculation valve opening is lesser for the HEM than the Bernoulli model. This result is in agreement with the static simulation experiment. Provided we have the necessary sensor requirements, HRS using HEM model is better suited for efficient operation of the pumps. However, at this point of time it is not clear if a densitometer will be available to measure density at pump inlets (mandatory for HEM). Also, solving for mass flux in 4-4-2-4 is cumbersome as it extensively needs PVT (pressure, volume and temperature) tables. Therefore, for minimum flow control the HRS strategy using the Bernoulli model is implemented. In further references, HRS refers to the High Robustness Strategy which makes use of the Bernoulli model.

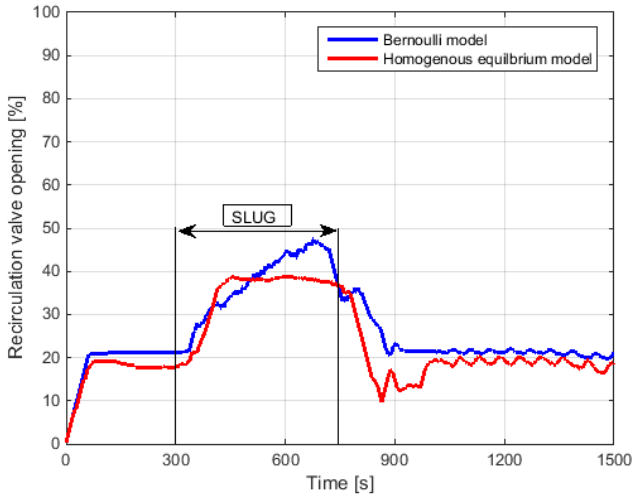

Figure 4-20: Valve opening comparison for Bernoulli and HEM in the presence of 7 minute slug.

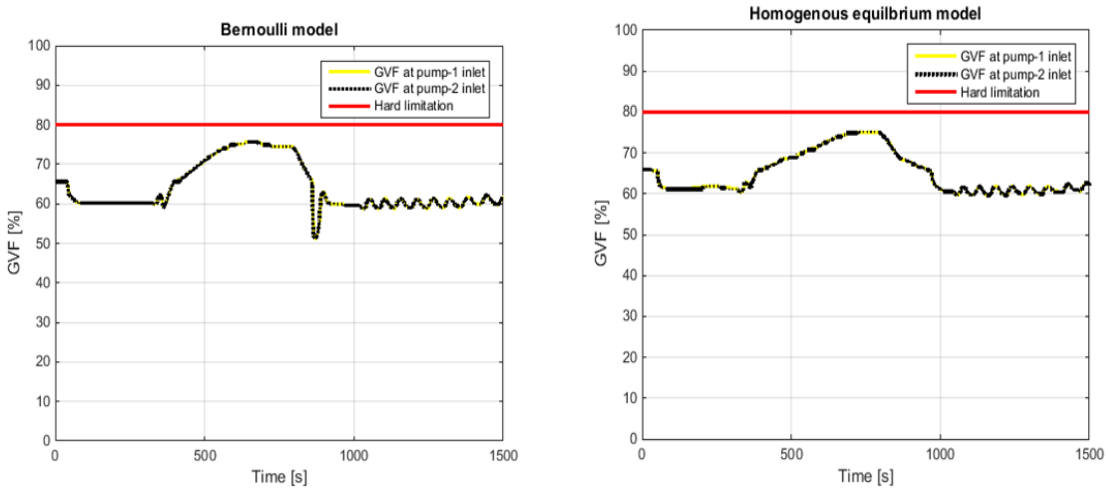

(a) HRS using Bernoulli model. **(b)** HRS using HEM.

Figure 4-21: GVF at pump inlet for Bernoulli and HEM

4-4-3 Production comparison

In this section, the production due to the HRS is compared with respect to the baseline strategy. Two different constant valve openings are chosen for the baseline strategy: Baseline-1 (40% opening) and Baseline-2 (20% opening). The master controller and load sharing controller are run commonly to both, the baseline and HRS.

For all the strategies, the system was brought to a steady state and same initial pump speeds were set. A 3 minute reservoir slug was introduced at the 300th second of a 25 minute long simulation. All the three strategies enabled the MPPs to survive the slug and also ensured that the GVFs at the inlet of the pumps were below 80%. The recycle valve openings due to the three strategies are shown in Fig. 4-22. The production increase obtained by the HRS and Baseline-2 with respect to the Baseline-1 is shown in Table 4-2.

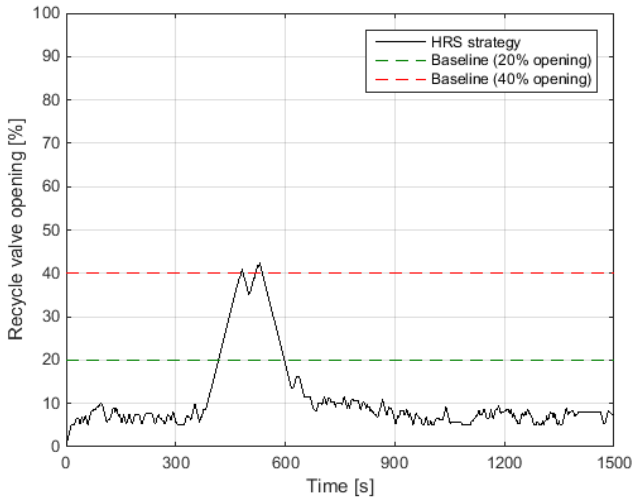

Figure 4-22: Valve opening comparison for Bernoulli and HEM in the presence of 7 minute slug.

Table 4-2: Relative increase in production wrt Baseline-1

	Baseline-1 (40% open)	**Baseline-2 (20% open)**	**HRS**
Production increase	N.A.	4.58%	8.12%

From Fig. 4-22 it can be noticed that the Baseline-1 strategy with 40% opening is the most conservative strategy. Out of the three, the HRS is the least conservative strategy as the recycle valve opening due to this strategy is the least. From Table 4-2 it is evident that the production obtained is maximum for the HRS. The reason for maximum production due to HRS is that, due to the lower recycle valve opening, the fluid mixture used in recycling is less and most of it passes through the risers to the top-side facility. Since the fluid recirculation is minimized, the effort on the pumps is also reduced in the long run thereby making the HRS the most efficient strategy.

Note: The recirculation valve opening is greater for the HRS than the baseline strategies during the slugs. But this period doesn't largely affect the production since the slugs are composed only of gas packets. In the remaining duration, the valve opening is lesser for HRS thereby resulting in greater production.

4-4-4 High performance strategy (Future work)

The High Performance Strategy (HPS) is also a minimum flow control strategy. But in addition to minimum flow control, the HPS performs GVF control separately (unlike baseline and HRS) because in this strategy we assume GVF measurement is available from a multiphase flowmeter (MPFM). The HPS is expected to be the most efficient strategy for operation of the pumps.

In the HPS, the current volume flow is calculated online based on the pump maps using pump speeds, pump inlet GVF and volume flow. The set-point for control is then calculated online by adding a margin on the minimum flow as given by:

$$SP = (K1 + K2 \cdot GVF_{pi} + K3 \cdot v_p)v_{min}, \tag{4-22}$$

where SP is the control set-point, v_{min} is minimum volume flow in [m^3/s], $K1$ is a margin on volume flow, $K2$ is a margin on GVF, $K3$ is a margin on pump speed, GVF_{pi} is GVF at pump inlet.

While in the HRS we control the recirculation valve opening independent of current GVF, in the HPS we have a separate control loop for the GVF. The valve opening is dictated by both the control loops that is, minimum flow and GVF. Measurement of the pump inlet GVF obtained by a multiphase flow meter sensor (MPFM) is used to control the GVF to a certain set-point using a PID controller. The set-point is either computed online using a moving average of the GVF or by the average GVF of the mixture from the reservoir.
Simulations with the HPS on the co-simulation environment are to be investigated in the future.

4-4-5 Summary of the minimum flow control strategies

The three minimum flow & GVF control strategies are summed up in brief in this section.

- **Baseline Strategy:** Constant opening of the recirculation valve independent of GVF and pump speed and other current operating conditions. Maximum recirculation in the system. Least production is obtained.
- **HRS:** Recirculation valve opening based on static pump maps, pump speed and differential pressure Opening independent of current GVF. Minimum recirculation in the system. Results in more production.
- **HPS:** Recirculation valve opening actively controlled based on pump speed, volume flow and GVF. Recirculation only when required. Expected to be the most effective and productive strategy.

The valve opening surfaces of the three strategies are shown in Fig. 4-23. These three strategies are further compared in terms of sensors, efficiency and implementation in Table 4-3.

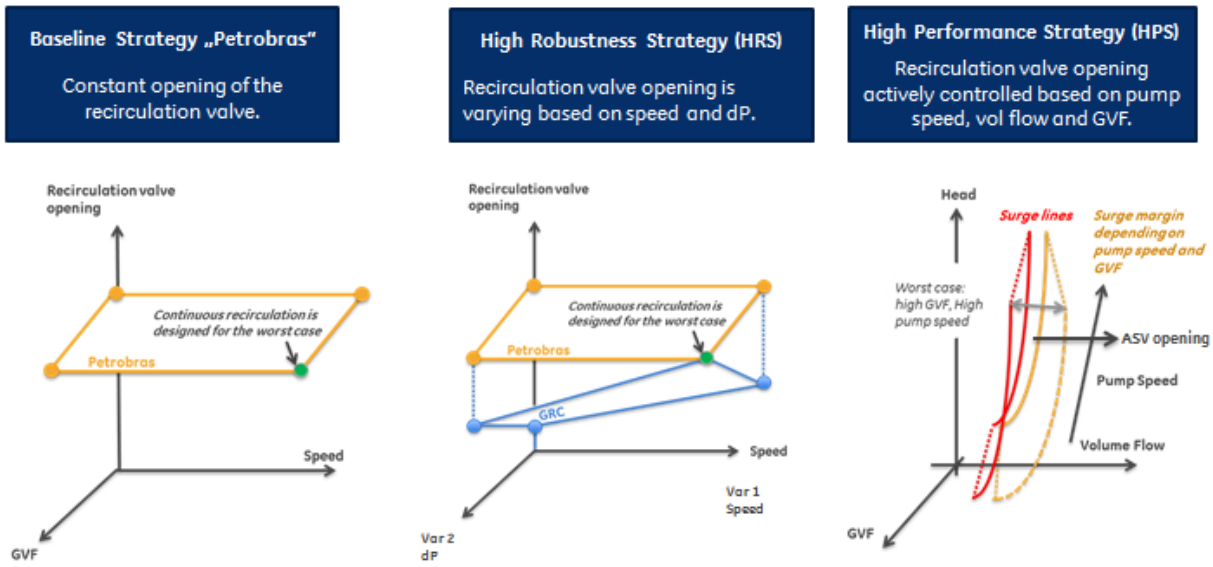

Figure 4-23: Valve opening based on the three minimum flow control strategies.

Table 4-3: Comparison between baseline strategy, HRS and HPS

	Baseline	HRS	HPS
Sensors	Only basic sensors	Intermediate no. of sensors	High no. of sensors
MPFM	Nil	Nil	One at mixer outlet
Implementation	Easy	Low computational effort	Complex
Efficiency	Least	Intermediate	Highly efficient

4-5 Riser slugging control

4-5-1 The riser slugging problem

Slugging in production risers has for many years been a major operational problem in subsea oil and gas fields developments. The slug is first initiated by liquid accumulating at the bottom of the riser blocking the gas to pass through. The liquid starts to fill up the riser, while the gas pressure in the bottom pipeline starts to build up. Often the liquid column fills up the whole riser before the gas pressure overcomes the hydrostatic pressure in the riser. When this happens, the slug is pushed out of the riser with an accelerating speed. While the liquid is being pushed out of the riser, the pressure starts to fall in the riser causing the gas to expand. This causes an even bigger force pushing out the slug. After the slug is blown out, the pressure in the pipeline falls and the liquid starts accumulating at the bottom of the riser again [26]. The slugging in risers is exhibited by oscillating production from the riser.

Possible reasons for riser slugging are:

- Geometry of the pipeline, which allows for accumulation of liquid (oil/water) at the riser bottom.
- Low liquid and gas rates: High liquid and gas rates would mean more kinetic energy in the system. This also explains why slugging often is a larger problem at tail-end production of oil and gas fields.
- Choke valve opening also comes in to play whether slug flow is introduced or not. A lower valve opening increases the pipeline pressure, and also increases the differential pressure over the riser. This differential pressure must be larger than the hydrostatic pressure at all time to avoid slug flow to arise.
- The gas to oil ratio: The gas has a much lower density than the oil phase. If the gas to oil ratio is large, it implies that the density of the total flow is low compared to the case where gas to oil ratio is small. A larger gas to oil ratio implies that the system would be more resistant against slug flow.

4-5-2 Control strategy

Control of the top-side choke is considered out of scope in this work. An alternative control strategy using differential pressure set-point to control pump speed was developed to prevent slugging in the downstream riser. In order to mitigate slugging the following approach has been proposed: Calculate the required discharge pressure to push the column of liquid (weight of the liquid) up to the top of the riser. Subsequently, slugging in the downstream riser is eliminated by controlling the pump speed so as to maintain required discharge pressure at pump outlet. We ensure that the differential pressure across the riser is always larger than the hydrostatic head in the riser by setting the control set-point large enough. A discrete PID controller is used to control to the differential pressure set-point Δp_{set} in [bar] using the following equation:

$$\frac{v_p}{p_{d_{set}} - p_d} = P + I \cdot T_s \cdot \frac{1}{z-1} + D \cdot \frac{N}{1 + N \cdot T_s \cdot \frac{1}{z-1}}, \tag{4-23}$$

where v_p is pump speed in [rpm], p_d is discharge pressure in [bar], P is proportional gain, I is integral gain, D is differential gain, T_s is sampling time and N is the filter coefficient.

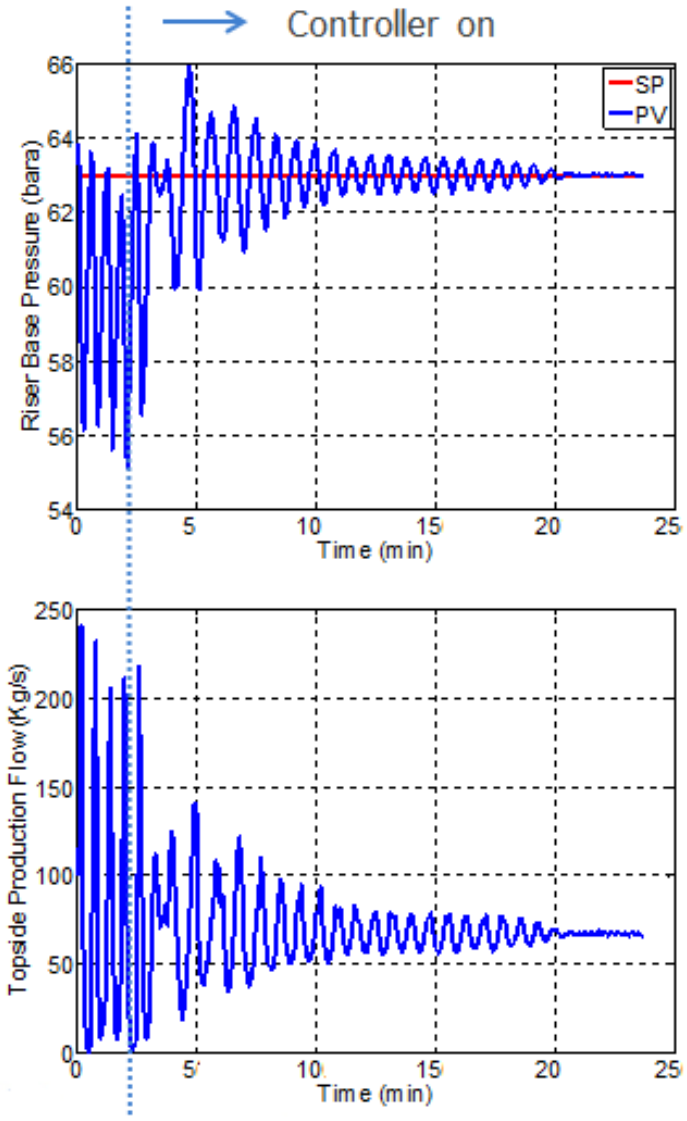

Figure 4-24: Production stabilization by anti-slug controller

In Fig. 4-24 the stabilization of production by controlling the discharge pressure (riser base pressure) to set-point is demonstrated. The discharge pressure converges to its set-point in 20 minutes duration and subsequently the production is also stabilized in the 20th minute. Note that, the initial oscillations in Fig. 4-24 correspond to slugging in the riser. These oscillations are suppressed over time and thus the slug is alleviated.

The anti-slug control for downstream slugging, together with HRS controller for pump safety, was tested as shown in Fig. 4-25

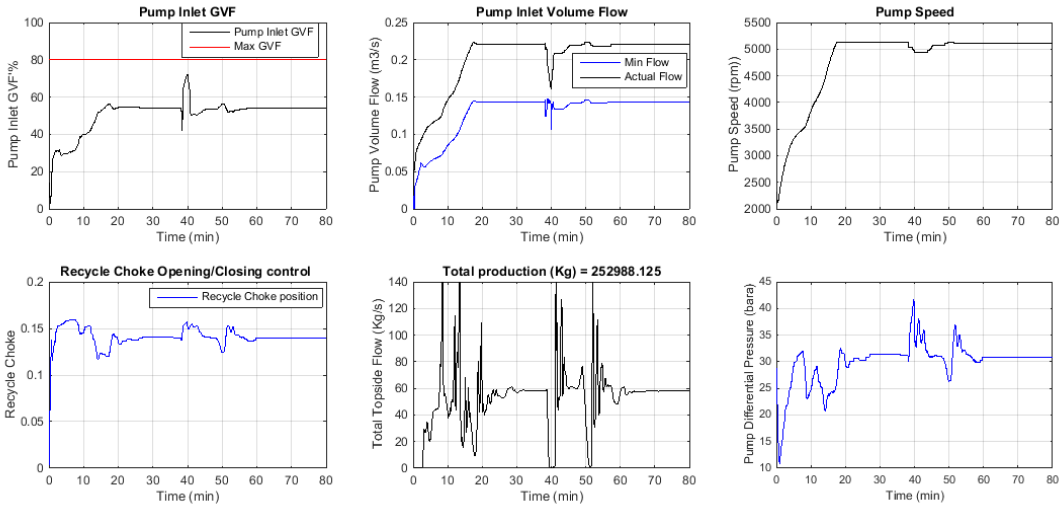

Figure 4-25: Results obtained by testing anti-slug controller together with HRS controller.

In Fig. 4-25 from the plot for pump inlet GVF, it can be observed that the GVF at pump inlet is below the hard limitation. Also, the volume flow into the pump is greater than minimum flow specified. Thereby, from the GVF and volume flow limits it is ascertained that pump safety is ensured. Further in Fig. 4-25 from the plot for pump speed and total production one can observe that steady state is reached after 20 minutes and the anti-slug controller has stabilized production in the downstream riser. Due to existing couplings between the controller for demand and load sharing, the anti-slug controller is tuned very conservatively. Thus, it takes as much as 20 minutes to stabilize production. In the 20th minute an inlet slug of 2 minutes duration was introduced. From the total production plot it can be observed that again in the 60th minute the anti-slug controller has stabilized production from the riser post the slug.

Chapter 5

Worst Case Scenario and Sensitivity Analysis

The controllers designed in Chapter 4 are to be tested in the most adverse conditions the boosting station might face. In this chapter, the worst case is identified by simulation experiments and then the controllers are tested.

When the controllers are implemented in real time, there are bound to be delays from the sensor measurements to the controllers and from the control signals to the process. The working of the controllers are to be tested in the presence of delays. Also, since the whole system is discrete, the system and controllers' functioning are to be examined by varying the sampling time.

5-1 Worst case determination

The system does not necessarily operate under ideal conditions. Ideal conditions would be same initial conditions for both the pumps. That is, the initial pump speeds are same, same volume flow into the pumps and the GVF at each of the pumps' inlet is the same. However, the system is prone to a number of uncertainties (disturbances) as listed in 1-3. This causes the initial pump conditions to be different.

In order to determine the worst case scenario for differences in GVF across the pumps and volume flow at the inlet of each pump, we vary the possible parameters in the K-Spice set-up which could typically induce the differences. These parameters are varied in a range determined by persons with operator experience in pumps and gas turbines.

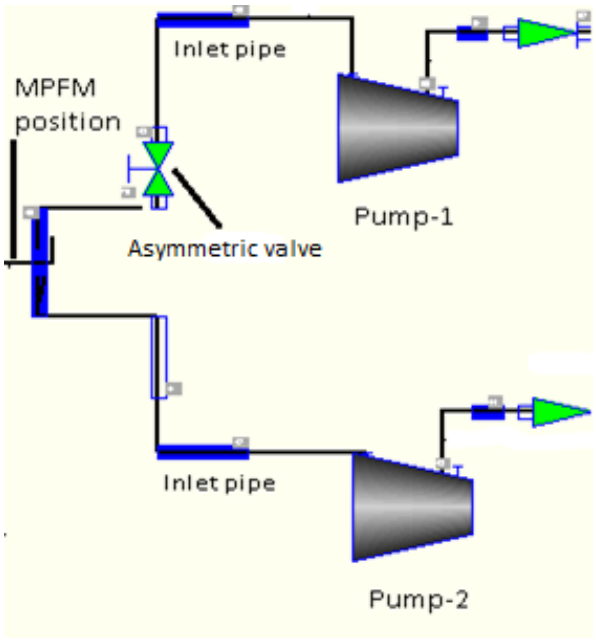

Figure 5-1: Asymmetric valve introduced in K-Spice model.

The possible parameters identified are: Relative height differences of the pumps, upstream inlet pipe diameter differences, inlet pipe length differences, different pump operational speeds and an asymmetric split between the pumps. In order to capture the asymmetric split, we introduce a valve in the K-Spice model (refer Fig. 5-1).

The differences in GVF and volume flow across the pumps by varying these parameters upto their maximum possible range is shown in Table 5-1.

Table 5-1: GVF and volume flow differences due to system uncertainties

Parameters	ΔGVF	ΔVF
Relative height differences of the pumps upto 1m	<1%	<1%
Upstream pipe diameter differences upto 50%	<1%	<1.5%
Inlet pipe length difference upto 5%	<1%	<1%
Operational pump speed differences upto 20%	<1%	<2%
Asymmetric split (including a valve opening upto 15%)	<17%	<7%

From Table 5-1 it can be observed that the worst case scenario is for an asymmetric split of reservoir flow across the pumps, leading to differences in GVF and volume flow upto 17% and 7% respectively. Therefore, for simulating the worst case scenario, we open the asymmetric valve by 15%.

In Fig. 5-2 the initial operating points of the MPPs in the worst case scenario are shown. The operating points are marked by a "★". As it can be seen from Fig. 5-2a and Fig. 5-2b the operating point of MPP-1 is much closer to the surge line (red line) than the operating point of MPP-2. From a control point of view this scenario poses a tough challenge where, the MPP-1 is likely to surge easily when the system is subject to reservoir slugs. For the sake of clarity, in 5-1-1 the simulation results of discharge pressure, surge margin and power consumed are plotted only for the MPP-1.

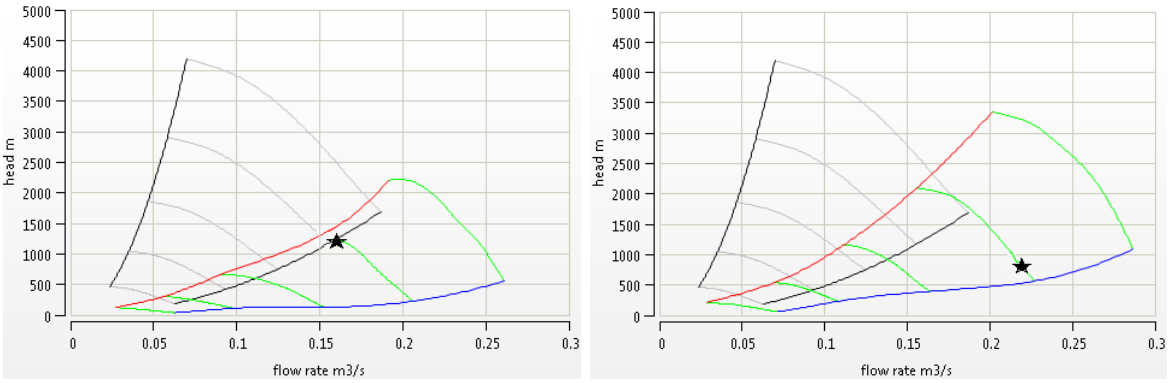

(a) Initial operating point of MPP-1. **(b)** Initial operating point of MPP-2.

Figure 5-2: Initial operating points of the MPPs in worst case scenario.

5-1-1 Worst case scenario simulation

In this section we test all the controllers designed for the boosting station and observe their performance for the worst case scenario. We also introduce 7 minute long slugs from both the reservoirs. For the minimum flow & GVF control, we test the baseline strategy and the HRS. Two different constant valve openings are chosen for the baseline strategy: Baseline-1 (20% opening) and Baseline-2 (40% opening). The results are shown in Fig. 5-3 and Fig. 5-4.

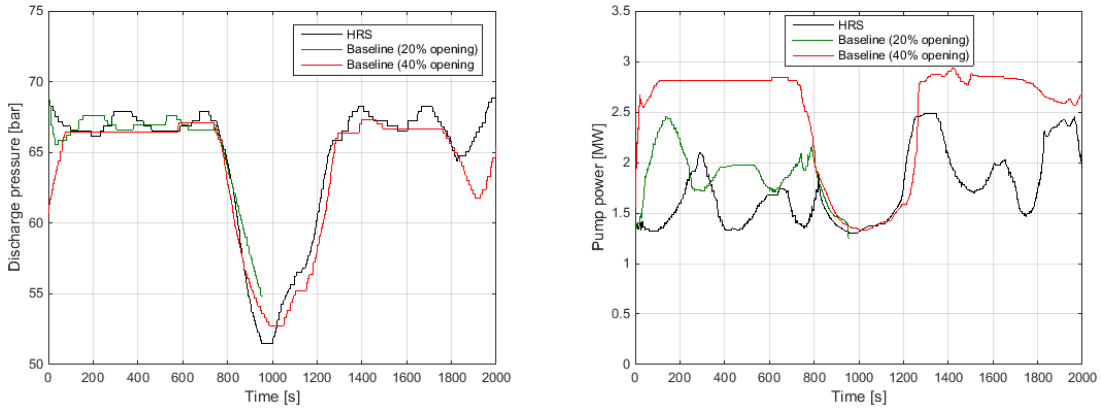

(a) Discharge pressure at pump outlet. **(b)** Power consumed by the pumps.

Figure 5-3: Master and load sharing controller results for baseline and HRS.

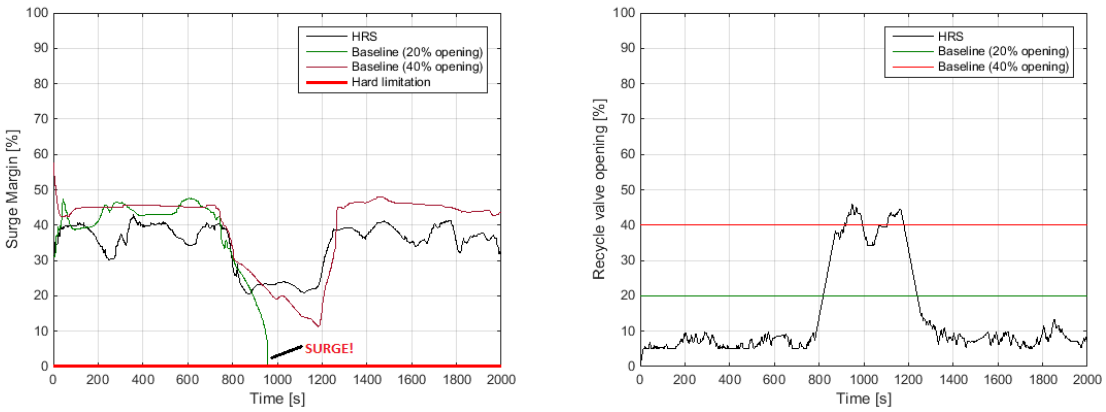

(a) Surge margin. **(b)** Recycle valve opening.

Figure 5-4: Minimum flow & GVF controller results for baseline and HRS.

The performance of the controllers in the worst case scenario are compared based on:

- Master controller: The master controller was assigned to control discharge pressure at the pump inlet to a set-point of 66 bar. For all the three strategies, the set-point was reached before the slug was introduced at the 800th minute (refer Fig. 5-3a). The discharge pressure has not yet converged to the set-point after the slugs, because of the lower gains of the PID controllers.
- Load sharing controller: The load sharing controller was able to distribute the load equally between the pumps (plot not shown). Also from Fig. 5-3b, we can observe that the power consumed was minimum for HRS.
- Minimum flow & GVF controller: For the minimum flow & GVF control, we tested using Baseline-1, Baseline-2 and the HRS. The recycle valve openings due to each of the three strategies are shown in Fig. 5-3a. All three strategies were able to limit the GVF at pump inlet to less than 80%. In order to test the minimum flow condition, the surge margin was plotted for the three strategies. The surge margin is typically the distance from the surge line. If the surge margin is zero it indicates that the pump has surged. As it can be observed from Fig. 5-4a the Baseline-1 (20% opening) could not handle the slugs. Baseline-2 and HRS were able to handle the slugs. However, since the valve opening is lesser for the HRS than the Baseline-2, the production and efficiency are expected to be more.

5-2 Sensitivity analysis

When we design a control system we need to account for all eventualities. For the boosting station, possibilities of delay in information communication exist. The controllers need to ensure safety even in presence of unforeseen delays. Also, the control system performance is to be tested for different choices of sampling periods. In this section, the controllers performance for different duration of delays and sampling periods is shown.

5-2-1 Delays

The transport delay block in Simulink is used to introduce input and output delays. Three sets of duration were chosen for the delays: 1, 5 and 10 seconds. The controllers were tested for the worst case scenario after implementing the delays. A 2 minute slug was introduced from the reservoirs at the 600th minute. For minimum flow & GVF control, the HRS was chosen. The controllers performance upon implementing the delays in shown in Fig. 5-5.

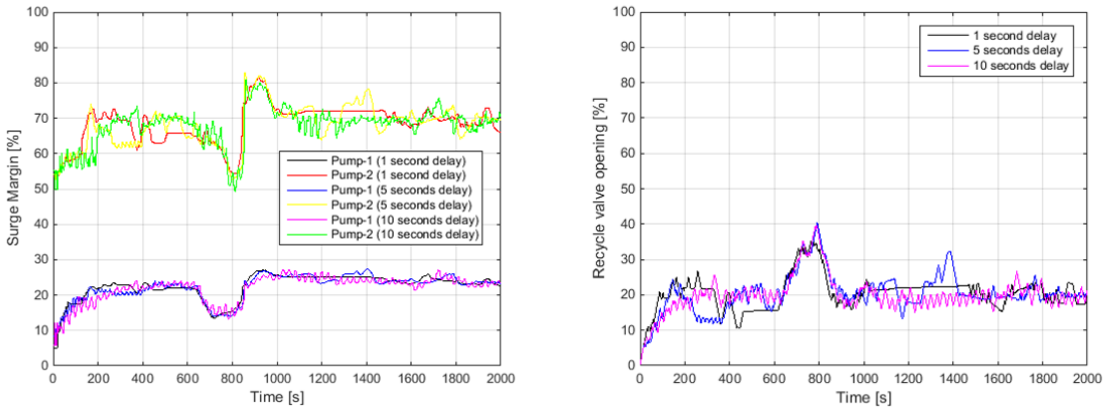

(a) Surge margin.

(b) Recycle valve opening.

Figure 5-5: Sensitivity Analysis: 1s, 5s and 10s delay

The discharge pressure was controlled to the set-point and load was balanced between the pumps. The valve openings for different delays are shown in Fig. 5-5b. Further, from Fig. 5-5a it can be seen that the surge margin of both the pumps does not reach zero for delay time of 1, 5 and 10 seconds. Therefore, we can conclude that the controllers perform well in the presence of delays.

5-2-2 Sampling time

The sampling period of the control system was varied in Simulink and the controllers performance was tested. Three sets of sampling time were chosen: 1, 2 and 3 seconds. The simulation results are in Fig. 5-6.

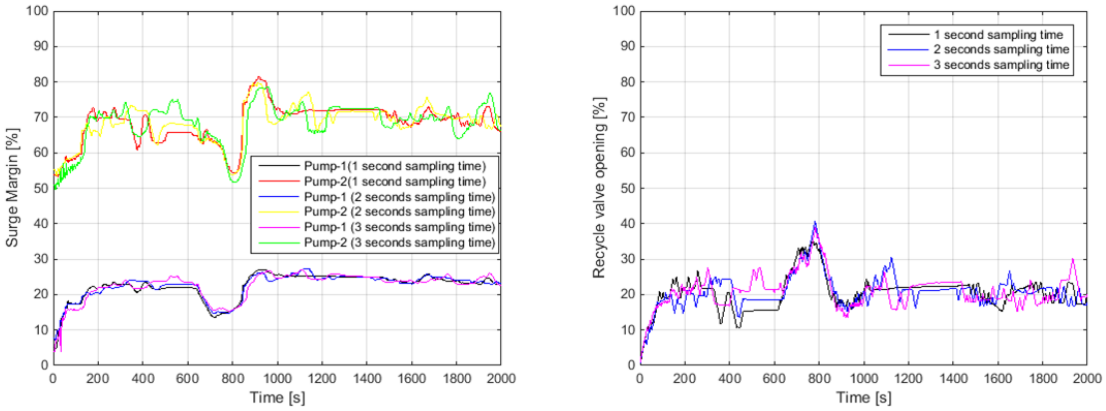

(a) Surge margin. **(b)** Recycle valve opening.

Figure 5-6: Sensitivity Analysis: 1s, 2s and 3s sampling time

The discharge pressure was controlled to the set-point and load was balanced. Even on the introduction of reservoir slugs, none of the pumps surged (refer Fig. 5-6a). Thus the controllers performance is satisfactory for the different sampling periods chosen.

Chapter 6

Conclusions and Future Scope

In response to the growing interest in multiphase boosting technology, GE has been working on the development of a subsea multiphase boosting station. In this work, the need for developing system level controls for the safe and reliable functioning of the boosting station was recognized. After establishing the control goals, a co-simulation environment was setup that enables design and validation of different control strategies in real-time against a high fidelity simulation model for the entire subsea production system from reservoir to topside choke.

Due to lack of sufficient sensors, the need to estimate some process parameters for control and monitoring was perceived. While the reservoir volume flow estimation produced desirable results, the GVF estimation still has ample scope for improvement. With sufficient information available, design of the controllers was the next objective.

Meeting the control goals, the controllers synthesized were:

- **Master control:** A PID control approach with desired set-point for the demand of the process variable was presented.
- **Load sharing:** Load sharing controller was designed to ensure that the load (reservoir flow) is balanced between the two multiphase pumps.
- **Minimum flow & GVF control:** Three strategies were developed to ensure that minimum flow into the pumps and maximal GVF at the pump's inlet are not violated. The three strategies were: Baseline, High Robustness Strategy (HRS) and High Performance Strategy (HPS). The strategies were distinguished based on sensor requirements, implementation difficulty, efficiency and expected production.
- **Riser slugging control:** In order to mitigate riser slugging and ensure constant production, an anti-slug controller was designed for the riser slugging phenomenon.

After determining the most adverse conditions the boosting station may face, the controllers were tested in the worst case scenario. The performance of the controllers matched the desired expectations. To conclude with, sensitivity analysis was done by implementing input-output delays and varying the sampling periods of the system.

Future work may include:

- Improving the GVF estimation algorithm after obtaining pump maps that have more data points for the lower GVF range.
- Testing the high performance strategy in the co-simulation environment.
- Developing the load sharing algorithm in such a way that recycle valve opening is also minimized.

Appendix A

Appendix A

A-1 Alternate method for GVF estimation

An alternative method for online GVF estimation from the model based on available measurements (differential pressure and pump speed) and the pump maps is proposed in this section. In this algorithm, at every instant sub map/maps are created based on the speed at which the pump is currently operating. Using the the sub map/maps, a distance factor is calculated which calculates distance from current operation point from all the data points in the map. Using the distance factor, GVF is estimated as explained in the subsequent section.

A-2 Online estimation using pump maps

The speed lines at which the pump is operated $\in \{2000, 3000, 4000, 5000, 6000\}$. The first step is to identify if the speed at which the pump is operating v_p (RPM) belongs to the speed lines. If $v_p \in$ speed lines then a sub map is created which contains all the data from the pump maps corresponding to that particular speed. A distance factor is calculated using the current power consumed by the pump P (MW) and differential pressure measured across the pump Δp_{mes} (Pa). The distance factor d is given by:

$$d(n) = \sqrt[q]{\left(\frac{\Delta p_{mes} - \Delta p_{map}(n)}{\Delta p_{mes}}\right)^a + \left(\frac{P - P_{map}(n)}{P}\right)^b} \qquad n = 1, 2, 3 \ldots N \tag{A-1}$$

where $q = \frac{a+b}{2}$, N corresponds to the number of data points in the sub map, Δp_{map} is differential pressure across the pump obtained from the sub map, P_{map} is the power consumed by the pump obtained from the sub map, a and b are scaling factors. The estimated GVF at the pump inlet is given as:

$$GVF_{est} = \frac{\sum_{n=1}^{N} \frac{1}{d(n)} GVF_{map}(n)}{\sum_{n=1}^{N} \frac{1}{d(n)}} \tag{A-2}$$

If pump speed v_p does not belong to the speed lines, then the upper and lower speed is identified from the speed range. Two sub maps are created for the lower and upper speed lines namely sub map low and sub map high. A distance factor is calculated for each of the two sub maps. The distance factor d_{low} is given by:

$$d_{low}(n) = \sqrt[q]{\left(\frac{\Delta p_{mes} - \Delta p_{low}(n)}{\Delta p_{mes}}\right)^a + \left(\frac{P - P_{low}(n)}{P}\right)^b} \qquad n = 1, 2, 3 \dots N \tag{A-3}$$

where $q = \frac{a+b}{2}$, Δp_{low} is differential pressure the pump for the sub map low and P_{low} is power consumed by the pump from the sub map low. The distance factor d_{high} is given by:

$$d_{high}(n) = \sqrt[q]{\left(\frac{\Delta p_{mes} - \Delta p_{high}(n)}{\Delta p_{mes}}\right)^a + \left(\frac{P - P_{high}(n)}{P}\right)^b} \qquad n = 1, 2, 3 \dots N \tag{A-4}$$

where $q = \frac{a+b}{2}$, Δp_{high} is differential pressure the pump for the sub map high and P_{high} is power consumed by the pump from the sub map high. Using the distance factors d_{low} and d_{high} we calculate the corresponding GVF's from the two sub maps using the following equations:

$$GVF_{low} = \frac{\sum_{n=1}^{N} \frac{1}{d_{low}(n)} GVF_{low}(n)}{\sum_{n=1}^{N} \frac{1}{d_{low}(n)}} \tag{A-5}$$

$$GVF_{high} = \frac{\sum_{n=1}^{N} \frac{1}{d_{high}(n)} GVF_{high}(n)}{\sum_{n=1}^{N} \frac{1}{d_{high}(n)}} \tag{A-6}$$

where GVF_{low} is GVF at pump inlet from sub map low and GVF_{high} is GVF at pump inlet from sub map high. Finally, the estimated GVF GVF_{est} will depend on both GVF_{low} and GVF_{high} as per the following equation:

$$GVF_{est} = \frac{(v_p - v_{low})GVF_{low} + (v_{high} - v_p)GVF_{high}}{v_{high} - v_{low}} \tag{A-7}$$

where v_p is the current pump speed, v_{low} is the lower speed line for the current pump speed and v_{high} is the upper speed line for the current pump speed.

This alternate algorithm too did not yield satisfactorily results for lower GVF range. The algorithm is to be improved after pump maps with more data points for lower GVF range are obtained.

Appendix B

Appendix B

B-1 Auto-coding from Simulink to PLC

While the various control algorithms are developed in Simulink, they need to be deployed in programmable logic controllers (PLCs) for hardware-in-the-loop validation. If the generation of PLC compatible code from Simulink to PLC is automated, it is helpful as: the human effort is reduced, the error due to human intervention is minimized and any changes in the Simulink model may be quickly reflected in the PLC code by using the auto-coding thereby alleviating the need for the human to re-do the whole code conversion again. Simulink PLC Coder generates hardware-independent structured Text from Simulink models, Stateflow charts, and MATLAB functions. The structured text is generated in PLCopen XML and other file formats supported by multiple IDE platforms including Rockwell Automation Studio which is under our consideration. As a result the Simulink applications can be compiled and conveniently deployed to numerous programmable logic controllers (PLCs). The procedure to use the Simulink PLC coder is as follows:

- Explicitly separate the blocks which have to be auto coded from the overall Simulink model. For example, if one needs to auto code the anti-slug controller alone, then a stand alone model of the anti-slug controller has to be made.
- Build subsystems containing the target blocks for auto coding. Please note that if the input to any block is obtained after an algebraic or any such operation, then that operation must also be included in the subsystem.
- Make sure to check the subsystem as an atomic unit. keep sampling time -1.
- Check the compatibility of the subsystem. If an error message is obtained then the user needs to refer to PLC coder official documentation. For example, possible source of errors are because some Simulink in built blocks like S-functions are not supported by the PLC coder and running K-Spice simultaneously.

- Set target IDE path before generating the code (Rockwell RSLogix 5000:AOI). Generate test bench data if needed.
- If report is required, the user should generate the traceability report.
- If the parameter values needs to be supplied as input by the user, the parameter values need to be defined in the Simulink using callbacks and PreLoadFcn (refer Fig. B-1) .
- Check the inline parameters box and select configuration option in the Optimization-signals and parameters window. Define the source as MATLAB workspace as shown in Fig. B-2 and add ImportedExtern to the storage class .

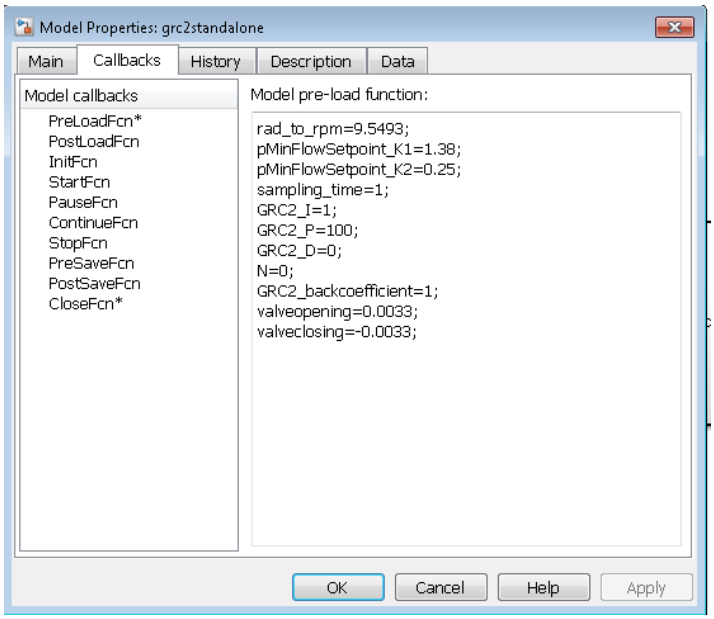

Figure B-1: Callbacks defined for input parameters.

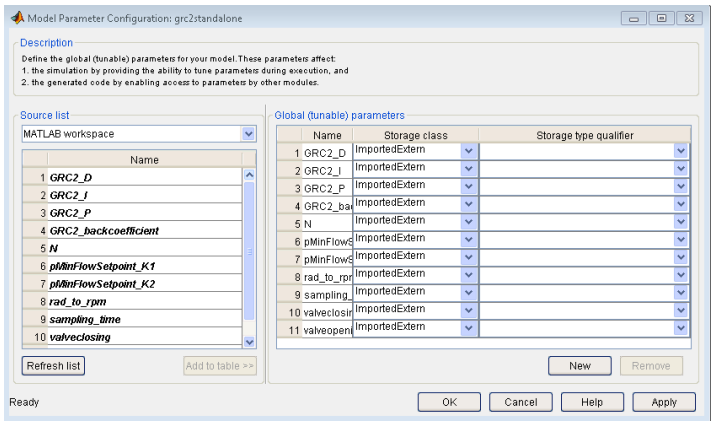

Figure B-2: Importing parameter values from MATLAB workspace.

Appendix C

Appendix C

C-1 Papers and patents in preparation

1. Manuscript on "Control of a subsea multiphase boosting station" to be submitted to the IFAC 2017 World Congress, Toulouse, France.
2. Patent application to be filed for the "HRS for the two pump configuration".

C-2 Presentation

1. Contributed in making a presentation on "Process control and operation of a subsea multiphase boosting station". The work was presented in the Subsea Valley Conference 2016, Oslo, Norway.

Bibliography

[1] Airam S., Paulo S., and Mauricio de Campos, "The slug flow problem in oil industry and pi level control." http://cdn.intechopen.com/pdfs-wm/40523.pdf. Accessed: 2016-01-22.

[2] Becquin G., Castane Selga R., Abrol S., Busboom A., Doder D., Jain A., Glomsaker T., Hyllseth M., and Ruigrok C., "Subsea multiphase boosting station system and controls optimization," *World Oil*, no. BHR-2015-J3, 2015.

[3] Nemoto R. H., Abrol S., and Becquin G., "Simplified model for control of severe slugging in s-shaped risers," *Offshore Technology Conference*, no. OTC-26110-MS, 2015.

[4] Jean F. and Sandrine D., *Multiphase Production: Pipeline Transport Pumping and Metering*. IFP Publications.

[5] "Production technology multiphase pumping - where to now?." http://www.offshore-mag.com/articles/print/volume-55/issue-5/news/production/production-technology-multiphase-pumping-where-to-now.html. Accessed: 2016-01-22.

[6] "Multiphase pumps: the path to success," *World Pumps*, vol. 2009, no. 511, pp. 18 – 20, 2009.

[7] Saadawi Hisham N.H., "An overview of multiphase pumping technology and its potential application for oil fields in the gulf region," *International Petroleum Technology Conference*, vol. IPTC-11720-MS, no. 6511, 2007.

[8] Falcimaigne J., Brac J., Charron Y., Pagnier P., and Vilagines R., "Pompage polyphasique : realisations et perpectives," *Oil & Gas Science and Technology - Rev. IFP*, vol. 57, no. 1, pp. 99–107, 2002.

[9] Gong H., Gioia F., Catalin T., and Gerald L. M., "Comparison of multiphase pumping technologies for subsea and downhole applications," *Oil and Gas Facilities*, February 2012.

[10] "Surge control considerations in centrifugal compressors." http://www.emersonprocessxperts.com/2010/04/surge_control_c/. Accessed: 2016-05-08.

[11] Woodward, "Advanced compressor load sharing algorithms,"

[12] Jahanshahi E., *Control Solutions for Multiphase Flow: Linear and nonlinear approaches to anti-slug control*. PhD thesis, Norwegian University of Science and Technology, 2013.

[13] Yehuda T., "Stability of severe slugging," *International journal Multiphase Flow*, vol. 12, no. 2, pp. 203–217, 1986.

[14] Balino J. L., Burr K. P., and Nemoto R. H., "Modeling and simulation of severe slugging in air-water pipeline-riser systems," *International journal Multiphase Flow*, vol. 36, pp. 643–660, 2010.

[15] Jansen F. E., Shoham O., and Taitel Y., "The elimination of severe slugging–experiments and modeling," *International journal Multiphase Flow*, vol. 22, no. 6, pp. 1055–1072, 1996.

[16] Yocum B. T., "Offshore riser slug flow avoidance: Mathematical models for design and optimization," no. SPE-4312-MS, 1973.

[17] Schmidt Z., Brill J.P., and Beggs H.D., "Experimental study of severe slugging in a two-phase flow pipeline riser-pipe system," *SPE journal*, vol. 20, pp. 407–414, 1980.

[18] Jahanshahi E., Skogestad S., and Lieungh M., "Subsea solution for anti-slug control of multiphase risers," *European Control Conference (ECC)*, 2013.

[19] "Matrikon." http://www.matrikon.com/drivers/opc/. Accessed: 2016-01-26.

[20] GE oil and gas, "Case study the schiehallion case," submitted, GE Internal.

[21] Rigzone, "How do risers work." http://www.rigzone.com/training/insight.asp?insight_id=308. Accessed: 2016-05-28.

[22] Guangshuo X., Simone S., Castane Selga R., Abrol S., Becquin S., and Busboom S., "Subsea multiphase boosting pump control strategy and simulink implementation," submitted, GE TISCAT report., 2015.

[23] FNW, "About cv," no. 3-2012, 2012.

[24] Kuchpil C., Souza C.E.M., Coelho E.J.J., Silva L.C.T., Cerqueira M.B. , and Carbone L., "Barracuda subsea helico-axial multiphase pump project," no. OTC-24217-PT, 2013.

[25] Ron D., "Size safety relief valves for any conditions," *Chemical engineering*, 2005.

[26] Einar Hauge, *Modeling and Simulation of Anti-slug Control in Hydro Experimental Multiphase Flow Loop*. PhD thesis, Norwegian University of Science and Technology, 2007.

Glossary

C-3 List of Abbreviations

- GVF - Gas volume fraction
- HEM - Homogeneous equilbrium models
- HDI - Homogeneous direct integration
- HPS - High performance strategy
- HRS - High robustness strategy
- MPP - Multiphase pump
- MPFM - Multiphase flow meter